Foldamer-Based Ultrapermeable and Highly Selective Artificial Water Channels that Exclude Protons

Arundhati Roy,[1,2,‡] Jie Shen,[2,‡] Himanshu Joshi,[3] Woochul Song,[4] Yu-Ming Tu,[4] Ratul Chowdhury,[5] Ruijuan Ye,[1] Ning Li,[2] Changliang Ren,[2] Manish Kumar,[6] Aleksei Aksimentiev[3] and Huaqiang Zeng[1,*]

[1] Institute of Advanced Synthesis, Northwestern Polytechnical University, Xi'an, Shaanxi 710072, China, and Yangtze River Delta Research Institute, Northwestern Polytechnical University, Taicang, Jiangsu 215400, China.

[2] NanoBio Lab, 31 Biopolis Way, The Nanos, Singapore

[3] Department of Physics and Beckman Institute for Advanced Science and Technology, University of Illinois at Urbana-Champaign, Urbana, IL, USA

[4] Department of Chemical Engineering, The University of Texas at Austin, Austin, TX, USA

[5] Laboratory of Systems Pharmacology, Harvard Medical School, Boston, MA, USA

[6] Department of Civil, Architectural and Environmental Engineering, The University of Texas at Austin, TX, USA

[‡] These authors contributed equally to this work. *Corresponding author email: hqzeng@nwpu.edu.cn (H.Z.)

General Remarks

All the chemicals were purchased from commercial sources and were used as received unless stated otherwise. Solvents were dried by standard protocols prior to use or purchased as dry. All chemical reactions were carried out under a nitrogen atmosphere. Thin layer chromatography (TLC) was carried out with silica gel coated plates and column chromatography was performed over silica gel (230-400 mesh) obtained from commercial suppliers. 18:1 (Δ9-Cis) PC or 1,2-dioleoyl-sn-glycero-3-phosphocholine (DOPC, 25 mg/mL), used to assemble stopped-flow LUVs, was purchased from Avanti Polar Lipids, USA. Egg yolk phosphatidylcholine (EYPC) lipid was also purchased from Avanti Polar Lipids as a solution dissolved in chloroform (25 mg/mL). All buffer solutions were prepared from MilliQ water and pH of the buffer solutions were measured using a Sartorius pH meter (PB-10). HEPES buffer, HPTS dye, SPQ dye, Triton X-100, NaOH and all inorganic salts of molecular biology grade were purchased from Sigma. Gel-permeation chromatography was performed on a column of Sephadex LH-20 gel (25 × 300 mm, V_0 = 25 mL). Large unilamellar vesicles (LUVs) were prepared from EYPC and DOPC lipid by using mini extruder, equipped with a polycarbonate membrane either of 100 nm or 200 nm pore size, obtained from Avanti Polar Lipids. Stopped-flow data was recorded by using SX20 Stopped Flow Spectrometer from Applied Photophysics equipped with a temperature controller (Polystat, Cole Parmer). Particle size (diameter) was measured using NanoBrook Omni Dynamic Light Scattering (DLS). Fluorescence was recorded using fluorescence spectrophotometer (Hitachi, Model F-7100, Japan). The ^{1}H and ^{13}C spectra were recorded on Bruker ACF-400 spectrometer using either residual solvent signals as an internal reference or from internal tetramethylsilane on the δ scale relative to dimethylsulphoxide-d_6 (δ 2.50 ppm) for ^{1}H NMR and ^{13}C NMR. The chemical shifts (δ) are reported in ppm. All fluorescence data were processed by Origin 8.5 and reaction schemes were prepared by ChemDraw Professional 15.0.

Synthetic Scheme

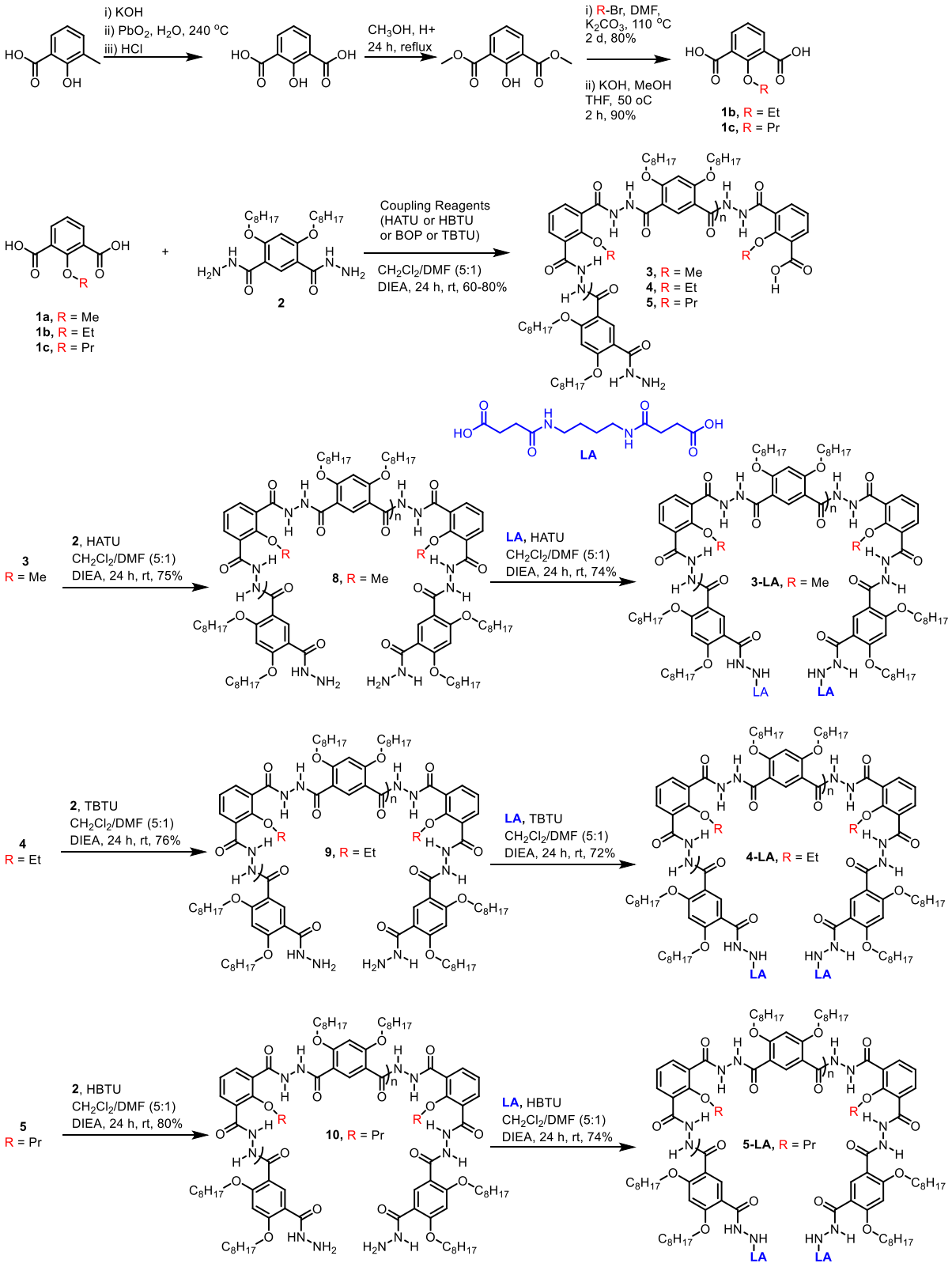

Supplementary Scheme 1. Reaction scheme for the synthesis of lipid anchor appended polymers (**3-LA, 4-LA** and **5-LA**) with three different alkoxy groups, with **8**-**10** and the most active polymers **3**, **4** and **5** as the intermediates.

Experimental Procedures:

Synthesis of compounds 1a-1c

2-methoxyisophthalic acid **1a** is commercially available and this compound was used directly for the next step.

2-hydroxyisophthalic acid was synthesised from 3-methylsalicylic acid following reported protocol and was esterified with CH_3OH in presence of catalytic amount of acid according to reported literature.[1] This dimethyl 2-hydroxyisophthalate was further alkylated with alkyl bromide (R-Br, R = C_2H_5 for compound **1b** and R = C_3H_7 for compound **1c**) in presence of K_2CO_3 and DMF. This reaction mixture was heated at 110 ^oC for 2 days and DMF was evaporated under reduced pressure. The reaction mixture was washed with excess amount of water to remove trace amount of DMF. The obtained crude product (10 mmol) subjected to ester hydrolysis without further purification in presence of KOH (5 equivalent) and CH_3OH/THF (1:1, each solvent of 15 mL) to obtain compounds **1b** and **1c**.

Compound **1b** (R = C_2H_5, yield = 90%) as white crystalline solid product. ^{1}H NMR (400 MHz, DMSO) δ 13.11 (s, 2H), 7.79 (d, *J* = 7.7 Hz, 2H), 7.24 (t, *J* = 7.7 Hz, 1H), 4.01 (q, *J* = 7.0 Hz, 2H), 1.27 (t, *J* = 7.0 Hz, 3H). ^{13}C NMR (101 MHz, DMSO) δ 167.31, 156.57, 133.41, 128.19, 123.63, 71.52, 39.52, 15.42.

Compound **1c** (R = C_3H_7) was also obtained as white crystalline solid product (yield = 93%). ^{1}H NMR (400 MHz, DMSO) δ 13.12 (s, 2H), 7.77 (d, *J* = 7.7 Hz, 2H), 7.23 (t, *J* = 7.7 Hz, 1H), 3.91 (t, *J* = 6.5 Hz, 2H), 1.68 (dd, *J* = 14.0, 6.6 Hz, 2H), 0.93 (t, *J* = 7.4 Hz, 3H). ^{13}C NMR (101 MHz, DMSO) δ 167.49, 156.59, 133.33, 128.20, 123.58, 77.28, 39.52, 22.97, 10.49.

Synthesis of compound 2: Compound **2** was synthesised according to the reported protocol.[2]

Synthesis of Polymers 3, 4 and 5[2]

In a 20 mL reaction vial, compound 4,6-bis(octyloxy)isophthalohydrazide (**2**, 0.118 mmol) and 2-alkoxyisophthalic acid (**1a**-**1b**, 0.118 mmol) were mixed. Coupling reagents (0.354 mmol) were added to each reaction vial. This was followed by adding freshly distilled CH_2Cl_2 (5 mL) and 1 mL DMF (dimethylformamide) in an N_2 atmosphere. 100 µL DIEA (N,N-Diisopropylethylamine) was then added in the reaction mixture, and the solution was stirred for 2 days at room temperature. After completion of reaction, solvent was evaporated to remove CH_2Cl_2 and DMF. The obtained residue was first washed with 10 mL MeOH/H_2O (1:1) and subsequently washed with 10 mL water and 10 mL MeOH and dried in oven (60 °C) to obtain polymers **3**-**5** as off-white solid powder with yields of 60 - 80%. Average molecular

weights (M_n) of all these polymers were determined by Gel Permeation Chromatography (GPC, Supplementary Tables 1 - 3).

HATU = 1-[Bis(dimethylamino)methylene]-1*H*-1,2,3-triazolo[4,5-b]pyridinium 3-oxid hexafluorophosphate

HBTU = *N,N,N′,N′*-Tetramethyl-O-(1*H*-benzotriazol-1-yl)uronium hexafluorophosphate

BOP = (Benzotriazol-1-yloxy)tris(dimethylamino)phosphonium hexafluorophosphate

TBTU = 2-(1*H*-Benzotriazole-1-yl)-1,1,3,3-tetramethylaminium tetrafluoroborate

Supplementary Table 1. GPC data for polymers **3** with R = CH_3.

Coupling reagent	**R = CH_3**		
	M_n	PDI	Channel Height
HATU	16.3 KDa	1.2	3.0 nm
HBTU	27.3 KDa	1.2	5.1 nm
BOP reagent	19.4 KDa	1.3	3.6 nm
TBTU	21.9 KDa	1.1	4.1 nm

Supplementary Table 2. GPC data for polymers **4** with R = C_2H_5.

Coupling reagent	**R = C_2H_5**		
	M_n	PDI	Channel Height
HATU	16.4 KDa	1.2	3.0 nm
HBTU	16.3 KDa	1.2	3.0 nm
BOP reagent	17.5 KDa	1.3	3.2 nm
TBTU	17.1 KDa	1.2	3.1 nm

Supplementary Table 3. GPC data for polymers **5** with R = C_3H_7.

Coupling reagent	**R = C_3H_7**		
	M_n	PDI	Channel Height
HATU	12.4 KDa	1.6	2.2 nm
HBTU	11.6 KDa	1.5	2.1 nm
BOP reagent	14.7 KDa	1.6	2.6 nm
TBTU	15.1 KDa	1.3	2.7 nm

Synthesis of Polymers 8-10

Polymer **3** made using HATU (0.018 mmol) and 4,6-bis(octyloxy)isophthalohydrazide (**2**, 0.06 mmol) were added to a 20 mL glass vial equipped with screw cap. HATU (0.07 mmol) was added in the same reaction vial. Freshly distilled CH_2Cl_2 (2.5 mL) and 0.5 mL DMF (dimethylformamide) was added to the reaction vial in presence of nitrogen atmosphere. This was followed by adding 100 µL DIEA (N,N-Diisopropylethylamine in the reaction mixture and stirred for 24 hours at room temperature. After completion of reaction, solvent was evaporated to remove CH_2Cl_2 and DMF. The obtained solid residue was washed with 5 mL MeOH/H_2O (1:1), and off-white precipitate was observed. The obtained precipitate was filtered and obtained solid product was washed with 5 mL H_2O and 5 mL MeOH respectively and dried in oven (60 °C) to afford polymer **8** as off-white solid powder with yields of 75%.

Polymer **9** and **10** were synthesised from polymer **4** made using TBTU as coupling reagent (yield 76%) and **5** made using HBTU as coupling reagent (yield 80%), respectively, following similar reaction protocol as discussed above.

Synthesis of lipid anchor (LA):[3]

To a solution of 1,4-diaminobutane (0.8 mL, 8 mmol), and DMAP (0.39 g, 3.2 mmol) in dichloromethane (20 mL), succinic anhydride (3.2 g, 32 mmol) was added , and the reaction mixture was stirred at room temperature overnight. White solid was formed, and filtration was performed to collect the solid. The crude product was mixed in acetone and subjected for sonication, then filtrated and dried in oven (60 °C) to afford **LA** as white solid product 1.72g (yield, 75%).

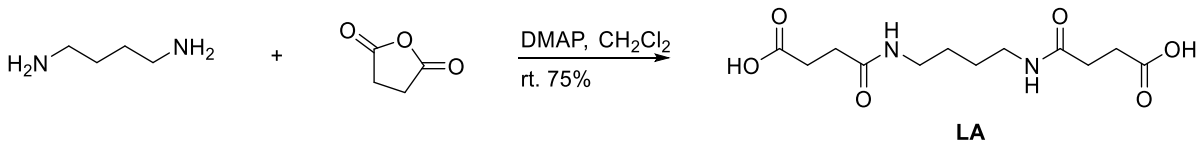

LA

Supplementary Scheme 2. Reaction scheme for the synthesis of lipid anchor (LA).

Synthesis of channels 3-LA, **4-LA and 5-LA:**

Polymer **8** (0.018 mmol) and **LA** (0.06 mmol) were mixed in a 20 mL round bottomed flask. HATU (0.07 mmol) was added in the same reaction vial. Freshly distilled CH_2Cl_2 (2.5 mL) and 0.5 mL DMF (dimethylformamide) was added to the reaction vial in presence of N_2 atmosphere. This was followed by adding 100 µL DIEA (N,N-Diisopropylethylamine in the reaction mixture and stirred for 48 hours at room temperature. After completion of reaction,

solvent was evaporated to remove CH_2Cl_2 and DMF. The obtained residue was washed with 5 mL MeOH/H_2O (1:1), and off-white precipitate was observed. The obtained solid precipitate was filtered and washed with 5 mL H_2O and 5 mL MeOH respectively to afford compound **3-LA** as off-white solid powder with yields of 74%.

Polymer **4-LA** and **5-LA** were synthesised from polymers **9** (using TBTU as coupling reagent, yield 72%) and **10** (using HBTU as coupling reagent, yield 74%), respectively, following similar reaction protocol as discussed above.

Supplementary Scheme 3. Synthetic scheme of trimer **6a**.

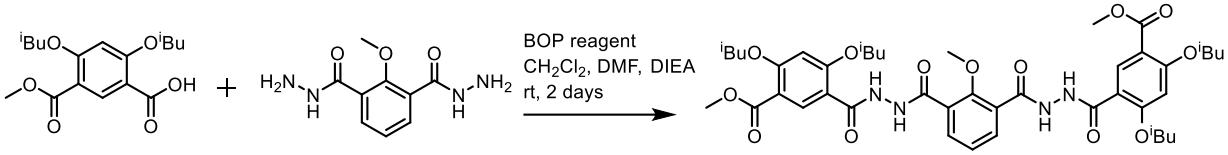

11 **12** **6a**

Synthesis of 2,4-diisobutoxy-5-(methoxycarbonyl)benzoic acid 11: Compound **11** was synthesized following the reported protocol.[4]

Synthesis of 2-methoxyisophthalohydrazide 12: Compound **12** was synthesized following the reported protocol.[5]

Synthesis of Trimer 6a (Trimer **6a** was made for crystal investigation shown in Supplementary Fig. 1b) In a 50 mL round bottom flask, 2,4-diisobutoxy-5-(methoxycarbonyl)benzoic acid (**11**, 1.00 g, 3.08 mmol) was dissolved in thionyl chloride (15 mL) and was refluxed for 3 h. Thionyl chloride was evaporated under reduced pressure to obtain the corresponding acid chloride derivative. 2-methoxyisophthalohydrazide **12** (346 mg, 1.54 mmol) was added, following by adding dry CH_2Cl_2 (dichloromethane, 25 mL) in a nitrogen atmosphere. 1.1 mL DIEA (*N,N*-Diisopropylethylamine) was then added in the reaction mixture, and the solution was stirred for 48 h at room temperature. After completion of reaction, CH_2Cl_2 was removed under reduced pressure. The obtained residue was purified through silica gel column chromatography (eluent: 1% MeOH in CH_2Cl_2), and off-white solid product **6a** was observed (791 mg, 61%). ^{1}H NMR (400 MHz, $CDCl_3$) δ 10.72 (d, *J* = 4.1 Hz, 4H), 8.79 (s, 2H), 8.27 (d, *J* = 7.8 Hz, 2H), 7.41 (t, *J* = 7.8 Hz, 1H), 6.48 (s, 2H), 4.17 (s, 3H), 4.02 (d, *J* = 6.6 Hz, 4H), 3.90 – 3.83 (m, 10H), 2.47 (dt, *J* = 13.3, 6.7 Hz, 2H), 2.23 (dd, *J* = 13.3, 6.6 Hz, 2H), 1.20 (d, *J* = 6.7 Hz, 12H), 1.11 (d, *J* = 6.7 Hz, 12H). ^{13}C NMR (100 MHz, $CDCl_3$) δ 165.2, 163.7, 161.4, 160.0, 159.2, 156.7, 137.1, 135.5, 125.6, 125.3, 113.3, 110.7, 96.7, 77.2, 76.6, 75.5, 64.9, 51.9, 28.5, 28.5, 19.7, 19.3.

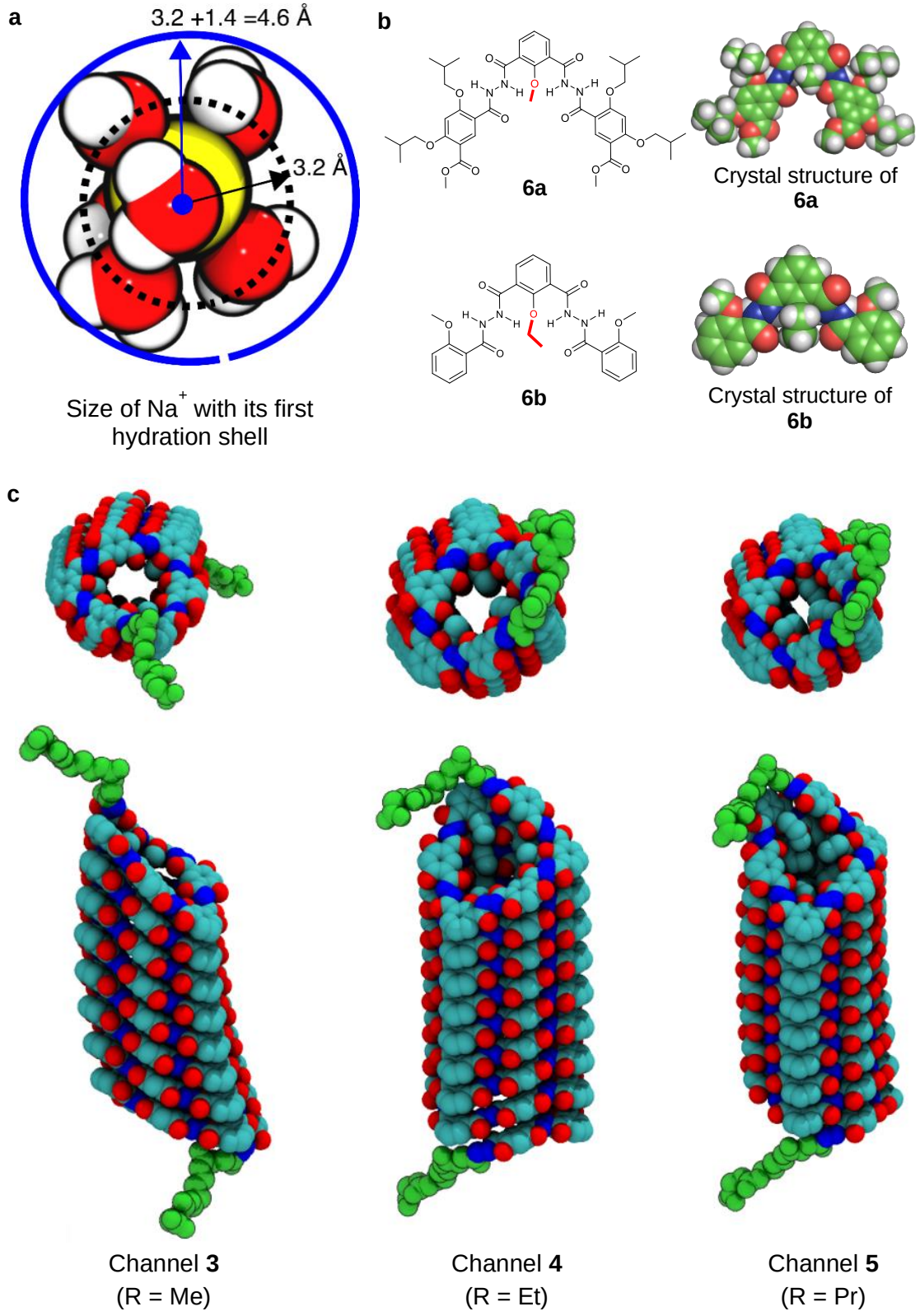

Supplementary Fig. 1 | Molecular size of a hydrated Na^+ ion, crystal structures of trimers 6a and 6b as well as top and side views of MD-simulated lipid anchor-modified channels 3-LA, 4-LA and 5-LA, each having 26 units 1 and 25 units 2 as well as a helical height of 2.9 nm. CCDC numbers for **6a** and **6b** are 2008964 and 2008965, respectively.

MALDI-TOF Distribution Patterns of channels 3 and 4

MALDI-TOF mass spectra were acquired with Bruker Ultraflextreme (Bruker Daltonik GmbH, Germany) equipped with Bruker smartbeam II 355 nm nitrogen laser with an accelerating voltage of 25 kV in the linear configuration. Mass spectra were measured by using the positive mode of mass spectroscopy using reported protocol.[2] The matrix used in the experiment was trans-2-[3-(4-tert-Butylphenyl)-2-methyl-2-propenylidene]malononitrile (DCTB) from TCI and used directly without further purification. Selection of the laser used for ionization was performed directly through the software and required no adjustments to the individual lasers. MALDI-TOF experiment was carried out for polymers **3** and **4** and instrument can detect up to 10,000 Da. Both compounds displayed characteristic mass pattern of repeating unit in the MALDI spectra. The interior of the helical channel is highly electron rich and therefore can bind with multiple metal ions such as Na^+ or K^+ ions to give rise to doubly or multiply charged species and all these peaks can be observed in the MALDI spectra (Supplementary Fig. 2).

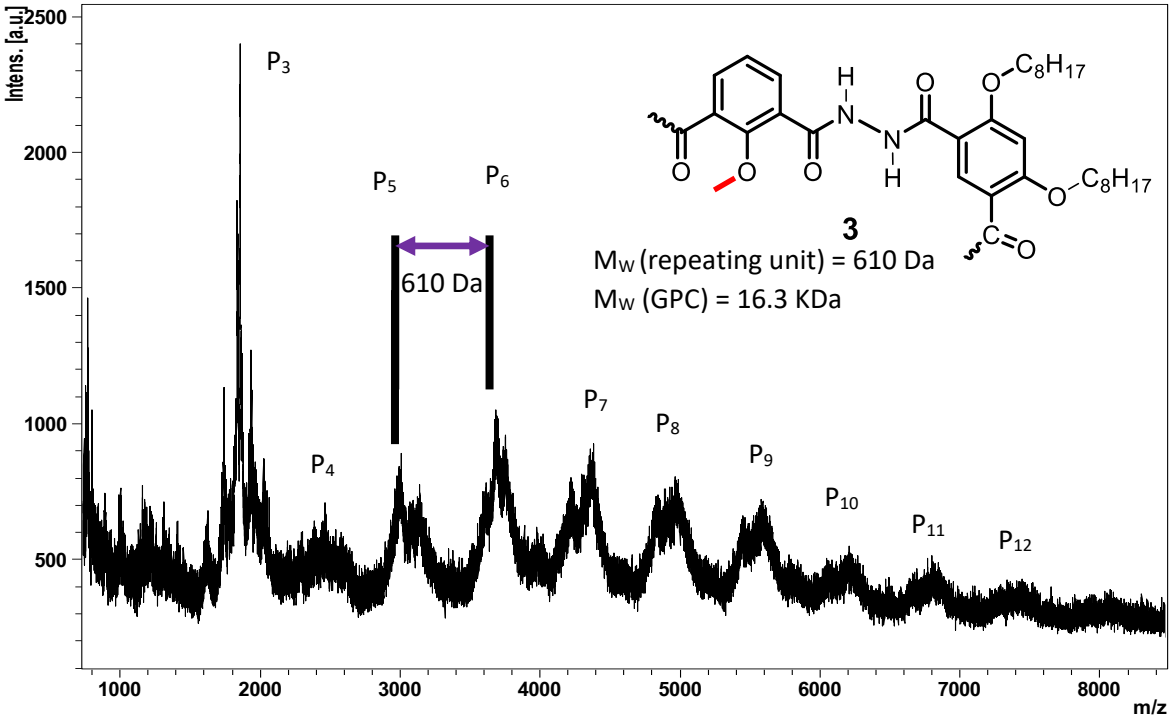

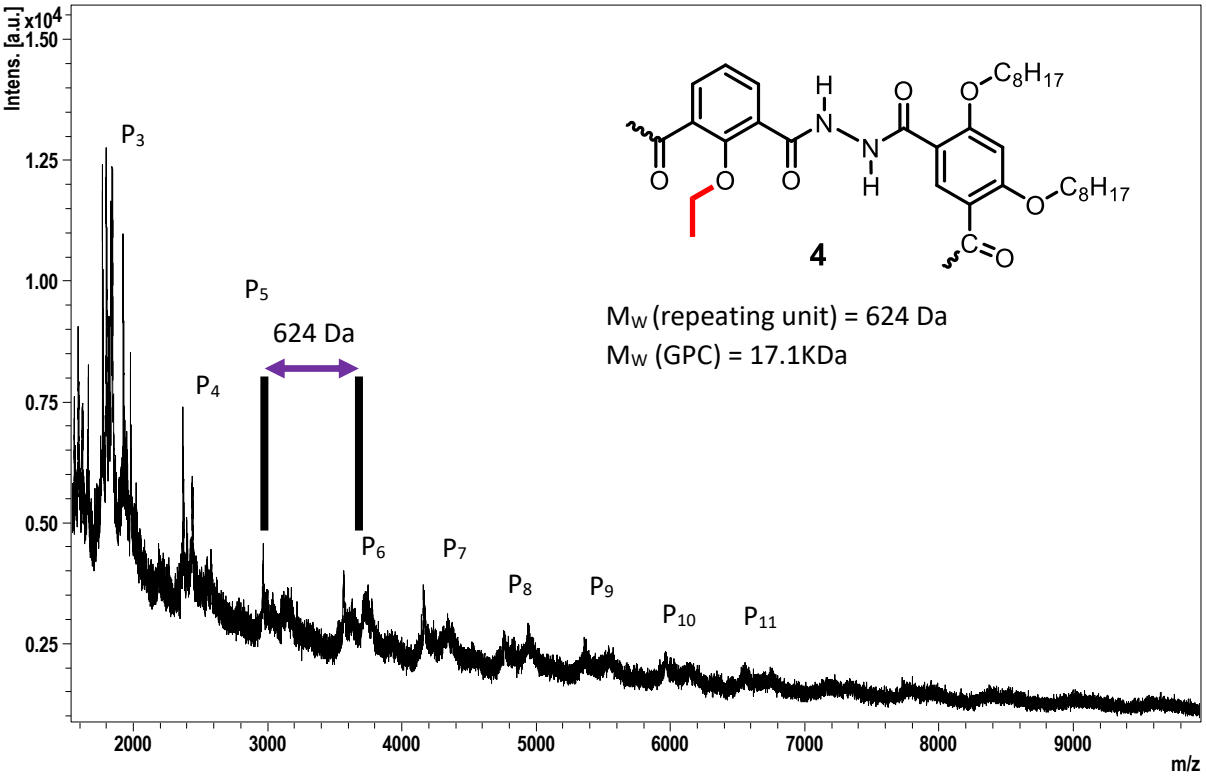

Supplementary Fig. 2 | MALDI-TOF patterns of polymers 3 and 4.

Protocol for Water Transport Study[6,7]

In 2 mL microtubes, 1,2-dioleoyl-sn-glycero-3-phosphocholine (DOPC, 0.24 mL) from Avanti Polar Lipids, USA (25 mg/mL in $CHCl_3$) and channel sample **3** made using HATU (dissolved in $CHCl_3$) were mixed at different molar ratios (1500:1 to 9000:1). The solvent was removed by Nitrogen flow and the resulting thin film was dried under high vacuum overnight. 1 mL HEPES buffer (10 mM HEPES, 100 mM NaCl, pH = 7.0) was then added into each microtube for hydration of lipid. In order to maximize incorporation extent of channel molecules into lipid membrane each microtube was vortexed for 30 s and sonicated for 2.5 min (37 kHz, power 100, 70 °C) for 10 cycles. If necessary, a glass spatula was used to scratch down all the lipid residue from the wall of microtube to minimize lipid loss and maximum channel incorporation. The lipid mixture was further subjected to 10 freeze-thaw cycles (freezing in liquid N_2 for 1 min and heating at 55^o C in water bath for 2.5 min). The lipid mixture was extruded at 80 °C for 15 times to obtain LUVs of 6 mg/mL concentration.

For stopped-flow experiment, this solution was diluted to 1 mg/mL with buffer (10 mM HEPES, 100 mM NaCl, pH = 7.0). LUVs were exposed to 3 different hypertonic solutions (0.3 M sucrose, 10 mM HEPES, 100 mM NaCl, pH = 7.0; 10 mM HEPES, 250 mM NaCl, pH = 7.0 or 10 mM HEPES, 100 mM NaCl, 150 mM NaCl, pH = 7.0). The abrupt decrease of the vesicle size could be observed due to transport of water to the extravesicular pool and this event leads to increase in light scattering intensity of 90° angle according to the Rayleigh-Gans theory. The changes of light scattering intensity caused by vesicle shrinkage were recorded at a wavelength of 577 nm and all these plots were fitted in the following form of single exponential function. [8 9]

$$y = A * exp(-kx) + y_o$$

where *y* = change in the light scattering, *k* is the exponential coefficient of the change in the light scattering end x is time.

Boyle-van't Hoff law says that change in the light scattering intensity is proportional to the change in the vesicle volume ($\Delta V/V_0$). Following this hypothesis, osmotic permeability (P_f) (in the unit of cm/s) was calculated according to the widely used equation as follow:

$$P_f = \frac{k}{\left(\frac{S}{V_0}\right) \times V_w \times \Delta C}$$

where *k* is the exponential coefficient of the change in the light scattering; *S* and V_0 are the initial surface area and volume of the vesicles, respectively; V_w is the molar volume of water, and Δ_{osm} is the osmolarity difference.

In order to calculate the true water permeability (*P_w* in the unit of cm^3/s) of water channels, the *$P_{f(blank)}$* value of the blank vesicle without water channel needs to be deducted from *$P_{f\ (channel)}$* which was multiplied by the vesical surface area (*S*) and divided by the number of water channels (*N*) incorporated in the liposome as shown below. Considering 100% incorporation of the water channels, the calculated *P_w* value can be calculated as below.

$$P_w = (P_{f(Channel)} - P_{f(blank)}) \times (\frac{S}{N})$$

The size of LUVs was determined by dynamic light scattering after 10 times dilution of the aforementioned LUVs solution (*i. e.* 1 mg/mL) with buffer (10 mM HEPES, 100 mM NaCl, pH = 7.0).

Re-calculation of water permeability using recently reported equation:[10 11 12]

$$P_f = \frac{k}{\left(\frac{S}{V_0}\right) \times V_w} \times \frac{C_{in,0} + C_{out}}{2{C_{out}}^2}$$

where $C_{in,0}$ and C_{out} are osmolyte concentration inside (initial, t = 0 s) and outside of vesicles, repectively.

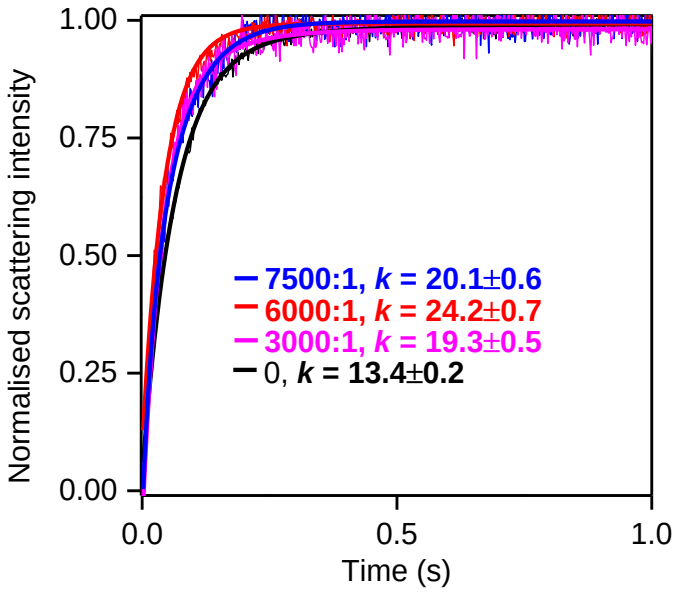

Supplementary Fig. 3 | Water transport curves of channel 3 (made using HATU) obtained using stopped-flow apparatus at different lipid to channel molar ratios. Exponential coefficients (k) were obtained by fitting the data into the equation of y = A*exp(-kx) + y0.

Supplementary Table 4. Water permeability (P_w) data for polymer **3** (made using HATU) and **4** (made using TBTU) at different channel to lipid ratio (1500:1 to 9000:1). ND = Not determined.

Lipid to channel ratio	P_w (10^{-14} cm^3/s) of **3**	P_w (10^{-14} cm^3/s) of **4**
1500	2.03 ± 0.49	6.07 ± 0.54
3000	3.19 ± 0.28	ND
4500	4.00 ± 0.74	ND
6000	7.75 ± 0.76	8.97 ± 0.39
7500	1.25 ± 0.35	ND
9000	-6.005 ± 0.13 [a]	ND

a, The background signal is even larger than the signal caused by the channel at this low channel density, leading to a negative value.

Supplementary Table 5. Water permeability (P_w) data for all polymers **3**, **4** and **5** at channel to lipid ratio of 6000:1.

3 (R = CH_3)		**4 (R = C_2H_5)**		**5 (R = C_3H_7)**	
Coupling agents	P_w (10^{-14} cm^3/s)	Coupling agents	P_w (10^{-14} cm^3/s)	Coupling agents	P_w (10^{-14} cm^3/s)
HATU	7.75 ± 0.76	HATU	6.01 ± 0.18	HATU	14.40 ± 1.34
HBTU	5.64 ± 0.95	HBTU	3.93 ± 0.28	HBTU	14.71 ± 0.97
BOP	6.62 ± 1.22	BOP	4.25 ± 0.31	BOP	14.26 ± 1.60
TBTU	6.18 ± 0.28	TBTU	8.97 ± 0.39	TBTU	13.43 ± 2.20

Determination of Insertion Efficiency[13]

In order to calculate insertion efficiency of the water channels in the lipid bilayer membrane, calibration curve was plotted. At first, blank LUVs (without any synthetic channels) were prepared from 3 mg/mL to 7 mg/mL concentration by using film rehydration method (except extrude) as discussed above. All these solutions were scanned on a UV-Vis spectrometer and UV absorbance was found to be decreased proportionally with decrease in concentration. Calibration curve was plotted using this UV-Vis data at 280 nm. Blank LUVs were also prepared by extruding through 200 nm membrane for 15 times to obtain monodispersed unilamellar vesicles with an initial concentration of 6 mg/mL which is equivalent to our experimental condition. UV absorbance was recorded with these extruded blank liposomes at 280 nm wavelength. The obtained data was used to get actual lipid concentration *i.e.* 4.4 ± 0.7 mg/mL and around 20% lipid was lost during extrusion process.

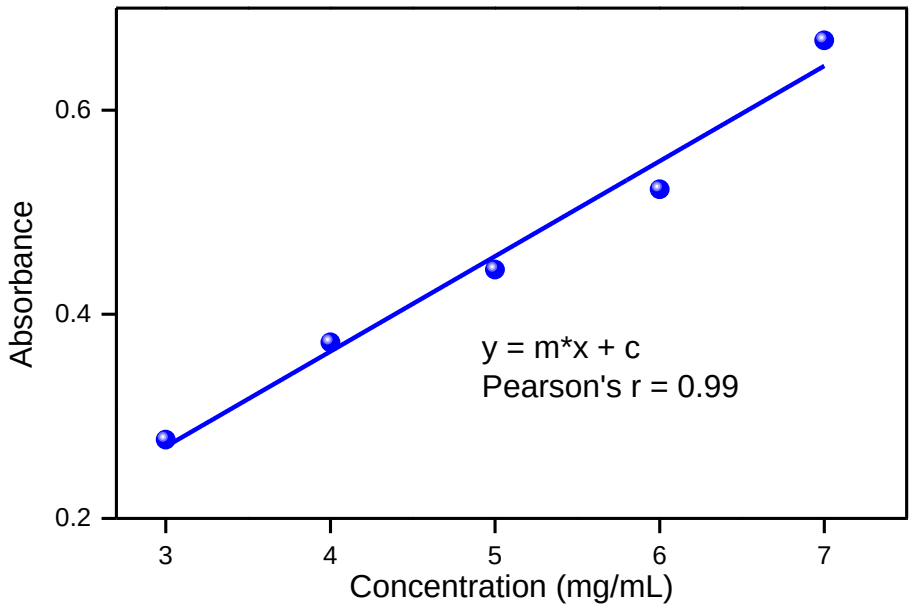

Supplementary Fig. 4 | The calibration curve obtained from UV-Vis absorbance of blank liposomes at different concentrations (3 mg/mL to 7 mg/mL). The data were fitted into the equation of y = mx + c where m = slope and c = intercept.

Since the concentration of synthetic water channels is extremely low as compared to lipid concentration in our experimental condition, the UV-absorbance plots of lipid superimpose the absorbance values of channels. Therefore, we have measured fluorescence spectra of the liposomes by incorporating water channels (λ_{ex} = 310 nm, λ_{em} = 430 nm). In these experiments, two separate batches of liposomes, embedded with artificial channels were prepared using film rehydration method as discussed earlier for each concentration ratio. One of the batches were not extruded and other batch was extruded through 200 nm membrane for 15 times to

obtain monodispersed LUVs. Fluorescence spectra was recorded for all these liposomes. Considering the lipid loss from the UV-Vis experiment and the ratio between fluorescence intensities (at λ_{em} = 430 nm) of non-extruded and extruded liposomes gives the value of insertion efficiency of the artificial water channels in the lipid membrane. The obtained insertion efficiency values were further used to calculate actual single channel water permeability of artificial water channels.

Supplementary Table 6. Insertion efficiency of AWCs **3-LA**, **4-LA** and **5-LA** in the lipid bilayer at different channel to lipid ratios. All data in the following table are average values from at least three measurements.

Molar ratio of Lipid : Channel	Insertion Efficiency of **3-LA**	Insertion Efficiency of **4-LA**	Insertion Efficiency of **5-LA**
4000	63 ± 2.4%	64 ± 1.3%	66 ± 4.5%
6000	66 ± 4.1%	72 ± 2.6%	75 ± 3.2%
8000	91 ± 1.2%	90 ± 2.2%	84 ± 1.2%
10000	96 ± 3.9%	93 ± 4.3%	94 ± 2.4%

Determination of Activation Energy[12]

To determine activation energies for water transport, water transport ability was measured by using stopped-flow instrument from 6 °C to 25 °C. For these experiments, temperature of the solution reservoir and the measurement cell of the stopped-flow instrument were maintained by a recirculating heater/chiller (Polystat, Cole Parmer). Permeability rates through artificial water channels at varying temperatures were fitted into the following Arrhenius equation to obtain activation energy (E_a).

$$\ln(k) = \ln(A) - \frac{E_a}{R}\left(\frac{1}{T}\right)$$

where *k* is the exponential coefficient of the change in the light scattering, *A* is Pre- exponential factor, E_a is Activation energy, R is Universal Gas constant and T is Absolute temperature.

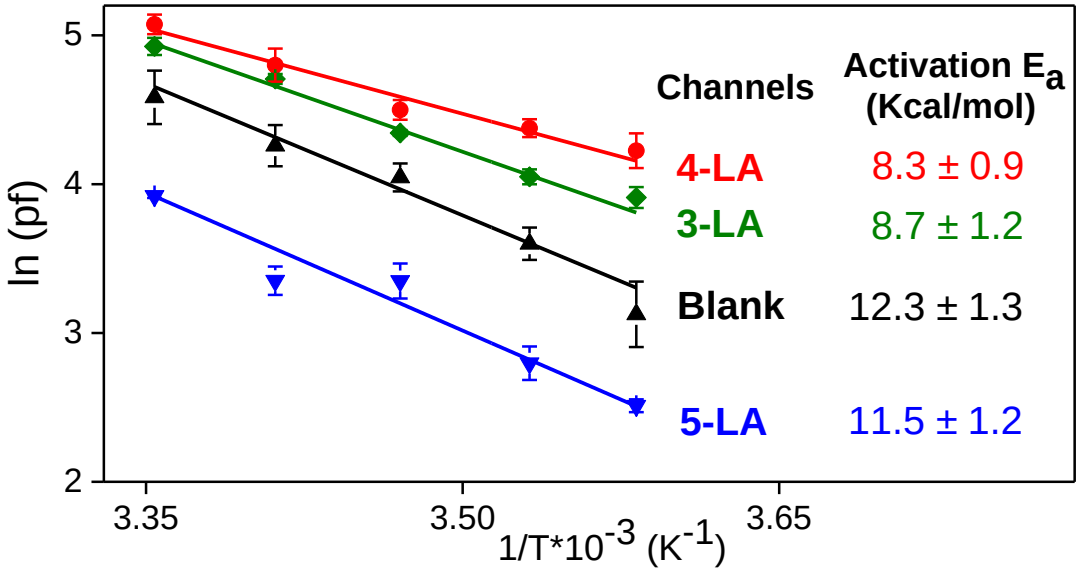

Supplementary Fig. 5 | Arrhenius plots of the water permeability as a function of temperature (6° to 25°C) for DOPC only (Blank), 3-LA, 4-LA and 5-LA for determining the corresponding activation energies (E_a) averaged over three runs.

Determination of Reflection Coefficients for 4-LA and gA

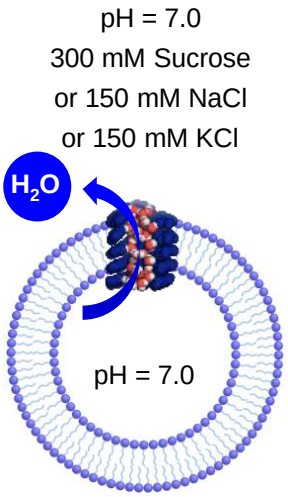

Reflection coefficient	Channels	
	4-LA	**gA**
$\frac{Pf\ (NaCl)}{Pf\ (sucrose)}$	1.03 ± 0.01	0.53 ± 0.02
$\frac{Pf\ (KCl)}{Pf\ (sucrose)}$	1.06 ± 0.01	0.07 ± 0.001

Supplementary Fig. 6 | Reflection coefficients of 4-LA vs gA (*i.e.*, ratio in water permeability determined using 300 mM sucrose, 150 mM NaCl or 150 mM KCl). The corresponding reflection coefficients are 1.03 ± 0.01 for P_f (NaCl)/P_f (sucrose) and 1.06 ± 0.006 for P_f (KCl)/P_f (sucrose), confirming that **4-LA** achieves nearly 100% rejection of NaCl and KCl. These approximate values can be corroborated by the low reflection coefficients of 0.53 ± 0.02 and 0.07 ± 0.001 for cation channel gramicidin A (gA), which is highly permeable to both Na^+ and K^+ ions, for NaCl and KCl respectively,

Ion Transport Activity using HPTS Assay

The HPTS assay for cation transport under high salt gradient: Egg yolk L-α-phosphatidylcholine (EYPC, 1 ml, 25 mg/mL in $CHCl_3$, Avanti Polar Lipids, USA) was placed in a 10 mL round bottomed flask and $CHCl_3$ was evaporated by purging N_2 slowly. After drying the resulting thin film under high vacuum overnight at room temperature, the film was hydrated with HEPES buffer solution (1 mL, 10 mM HEPES, pH = 7.0) containing a pH sensitive dye 8-hydroxypyrene-1,3,6-trisulfonic acid (HPTS, 0.5 mM) at room temperature for 1 hour (with occasional vortexing after every 15 minutes) to obtain a milky suspension. The mixture was then subjected to 10 freeze-thaw cycles (freezing in liquid N_2 for 1 minute and heating at 55 ^oC in water bath for 2 minutes). The vesicle suspension was extruded through polycarbonate membrane (0.1 μm) to produce a monodispersed large unilamellar vesicles (LUVs) of about 100 nm in diameter with HPTS encapsulated inside. The extravesicular HPTS dye was removed by using size exclusion chromatography (stationary phase: Sephadex G-50, GE Healthcare, USA, mobile phase: 10 mM HEPES buffer, pH = 7.0) and diluted with the mobile phase to yield 3.2 mL of 10 mM lipid stock solution.

30 μL of HPTS-containing LUVs was added to 1970 μL of HEPES buffer (10 mM HEPES, 200 mM M_2SO_4, pH = 8.0 where $M^+ = Na^+$ and K^+) in a clean fluorescence cuvette to generate salt gradient across lipid bilayer. This cuvette was placed on the fluorescence instrument (at t = 0 s) equipped with magnetic stirrer. Fluorescence emission intensity of HPTS dye, F_t was monitored at λ_{em} = 510 nm (λ_{ex} = 450 nm) with time. Channels of various types (1 μM, dissolved in DMF) were added at t = 70 s and recorded simultaneously for 300 seconds using fluorescence spectrophotometer (Hitachi, Model F-7100, Japan). Finally at t = 370 s, 20 μL of 20% Triton X-100 was added to destroy all vesicles which resulted in destruction of pH gradient to achieve the maximum change in fluorescence emission intensity of HPTS dye. Fluorescence data was also recorded for gramicidin A (gA, 0.1 μM) under same experimental condition and the obtained activity was compared with artificial water channels.

The time axis was normalized according to the following equation: $t = t - 70$. Fluorescence intensities (F_t) were normalized to fractional emission intensity I_F using following equation,

$$I_F = [(F_t - F_0)/(F_\infty - F_0)] \times 100$$

whereas F_0 = Fluorescence intensity just before the compound addition (at t = 0 s), F_∞ = Fluorescence intensity at saturation after complete leakage (at t = 300 s), and F_t = Fluorescence intensity at time t.

The HPTS assay for anion and proton transport study:[14] Egg yolk L-α-phosphatidylcholine (EYPC, 1 ml, 25 mg/mL in $CHCl_3$, Avanti Polar Lipids, USA) was taken in a 10 mL round

bottomed flask and $CHCl_3$ was evaporated by purging N_2 slowly. After drying the resulting thin film under high vacuum overnight at room temperature, the film was hydrated with 4-(2-hydroxyethyl)-1-piperazine-ethane sulfonic acid (HEPES) buffer solution (1 mL, 10 mM HEPES, 100 mM NaCl, pH = 7.0) containing a pH sensitive dye 8-hydroxypyrene-1,3,6-trisulfonic acid (HPTS, 0.5 mM) at room temperature for 1 hour (with occasional vortexing after every 15 minutes) to give a milky suspension. The mixture was then subjected to 10 freeze-thaw cycles (freezing in liquid N_2 for 1 minute and heating at 55 ^oC in water bath for 2 minutes). The vesicle suspension was extruded through polycarbonate membrane (0.1 μm) to produce a monodispersed large unilamellar vesicles (LUVs) of about 100 nm in diameter with HPTS encapsulated inside. The extravesicular HPTS dye was removed by using size exclusion chromatography (stationary phase: Sephadex G-50, GE Healthcare, USA, mobile phase: 10 mM HEPES, 100 mM NaCl and pH 7.0) and diluted with the mobile phase to yield 3.2 mL of 10 mM lipid stock solution.

30 μL of HPTS-containing LUVs was added to 1970 μL of HEPES buffer (10 mM HEPES, 67 mM Na_2SO_4, pH 8) in a clean fluorescence cuvette to generate pH gradient across lipid bilayer. This cuvette was placed on the fluorescence instrument (at t = 0 s) equipped with magnetic stirrer. Fluorescence emission intensity of HPTS dye, F_t was monitored at λ_{em} = 510 nm (λ_{ex} = 450 nm) with time. Channels (**3**, **4**, **5** and **L8**) or proton carrier (FCCP) at desired concentration in DMF were added at t = 70 s and recorded simultaneously for 300 seconds using fluorescence spectrophotometer (Hitachi, Model F-7100, Japan). Finally at t = 370 s, 20 μL of 20% Triton X-100 was added to destroy all vesicles which resulted in destruction of pH gradient to achieve the maximum change in fluorescence emission intensity of HPTS dye.

The time axis was normalized according to the following equation: $t = t - 70$. Fluorescence intensities (F_t) were normalized to fractional emission intensity I_F using following equation:

$$I_F = [(F_t - F_0)/(F_\infty - F_0)] \times 100$$

whereas F_0 = Fluorescence intensity just before the compound addition (at t = 0 s), F_∞ = Fluorescence intensity at saturation after complete leakage (at t = 300 s), and F_t = Fluorescence intensity at time t.

The SPQ assay for Anion transport:[15] Egg yolk L-α-phosphatidylcholine (EYPC, 1 ml, 25 mg/mL in $CHCl_3$, Avanti Polar Lipids, USA) was taken in a round bottomed flask and $CHCl_3$ was evaporated under reduced pressure at 30 ^oC. After drying the resulting film under high vacuum overnight at room temperature, the film was hydrated with a $NaNO_3$ solution (1 mL, 225 mM) containing a Cl^- sensitive dye 6-methoxy-N-(3-sulfopropyl)quinolinium (SPQ) (1 mM)

dye at room temperature for 1 hour (with occasional vortexing after every 15 minutes) to obtain a milky suspension. The mixture was then subjected to 10 freeze-thaw cycles: freezing in liquid N_2 for 60 seconds and heating at 55 ^oC for 2 minutes. The vesicle suspension was extruded through polycarbonate membrane (0.1 μm) to produce a homogeneous suspension of LUVs with SPQ encapsulated inside. The extravesicular SPQ dye was removed by using size exclusion chromatography (stationary phase: Sephadex G-50, GE Healthcare, USA, mobile phase: 225 mM $NaNO_3$ solution) and diluted with the mobile phase to yield 3.2 mL of 10 mM lipid stock solution.

The SPQ-containing LUV suspension (30 μL, 10 mM in 225 mM $NaNO_3$) was added to a NaCl solution (1.7 mL, 225 mM) to create an extravesicular chloride gradient. A solution of channel molecule **4-LA** (1 μM) in DMF at different concentrations was then injected into the suspension under gentle stirring. Upon the addition of channels, the emission of SPQ was immediately monitored at 430 nm with excitations at 360 nm for 300 seconds using fluorescence spectrophotometer (Hitachi, Model F-7100, Japan) after which time an aqueous solution of Triton X-100 (20 μL, 20% v/v) was immediately added to completely destroy the chloride gradient. The final transport trace was obtained by normalizing the fluorescence intensity using the following equation,

$$I_F = [(F_t - F_0)/(F_\infty - F_0)]$$

Where F_0 = Fluorescence intensity just before the compound addition (at t = 0 s), F_t = Fluorescence intensity at time t, and F_∞ = Fluorescence intensity at saturation after complete leakage (at t = 300 s).

Determination of Insertion Efficiency of AWC 4-LA for the HPTS assay:

Egg yolk L-α-phosphatidylcholine (EYPC, 1 ml, 25 mg/mL in $CHCl_3$, Avanti Polar Lipids, USA) was placed in a 10 mL round bottomed flask and $CHCl_3$ was evaporated by purging N_2 slowly. After drying the resulting thin film under high vacuum overnight at room temperature, the film was hydrated with 4-(2-hydroxyethyl)-1-piperazine-ethane sulfonic acid (HEPES) buffer solution (1 mL, 10 mM HEPES, 100 mM NaCl, pH = 7.0) at room temperature for 1 hour (with occasional vortexing after every 15 minutes) to give a milky suspension. The mixture was then subjected to 10 freeze-thaw cycles (freezing in liquid N_2 for 1 minute and heating at 55 ^oC in water bath for 2 minutes). The vesicle suspension was extruded through polycarbonate membrane (0.1 μm) to produce a monodispersed large unilamellar vesicles (LUVs) of about 100 nm in diameter. The LUV stock solution was diluted with the buffer (10 mM HEPES, 100 mM NaCl, pH = 7.0) to yield 3.2 mL of 10 mM lipid stock solution.

Three sets of fluorescence data were then recorded (Supplementary Fig. 7).

1. LUVs only: 30 μL LUVs was added to 1970 μL of HEPES buffer (10 mM HEPES, 100 mM MCl, pH = 8.0 where $M^+ = Na^+$ and K^+) in a clean fluorescence cuvette to generate a pH gradient across lipid bilayer. This cuvette was placed on the fluorescence instrument (at t = 0 s) equipped with magnetic stirrer. Fluorescence emission intensity was recorded (λ_{ex} = 310 nm , λ_{em} = 430 nm) using fluorescence spectrophotometer (Hitachi, Model F-7100, Japan).

2. Fluorescence data were recorded for **4-LA** (1 μM, DMF) with 30 μL LUVs under same experimental condition.

3. Fluorescence data were also recorded for **4-LA** (1 μM, DMF) without any LUVs and the obtained data were compared with other two data.

Compound **4-LA** (1 μM) is not soluble in HEPES buffer and precipitates out from the buffer solution. However, after insertion of **4-LA** (1 μM) in the bilayer membrane (Concentration of LUVs = 150 μM), precipitation was not observed. In this case, florescence intensity increased at least 3 times compared to LUVs without **4-LA** which consequently confirms insertion of AWCs in the membrane during ion transport studies using EYPC-LUVs. Blank sample (only LUVs) did not show any characteristic fluorescence emission in this wavelength range.

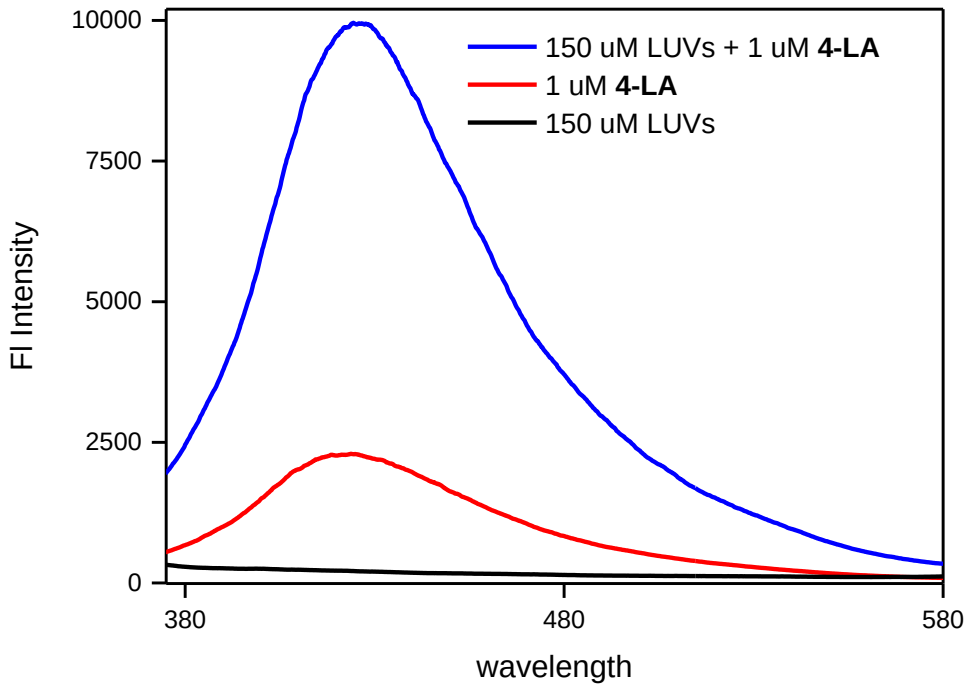

Supplementary Fig. 7 | Greater than 75% insertion efficiency of 4-LA (1 μM) in the bilayer membrane under the identical LUV-based assay condition by fluorescence emission spectroscopy.

Water Transport Selectivity Studies

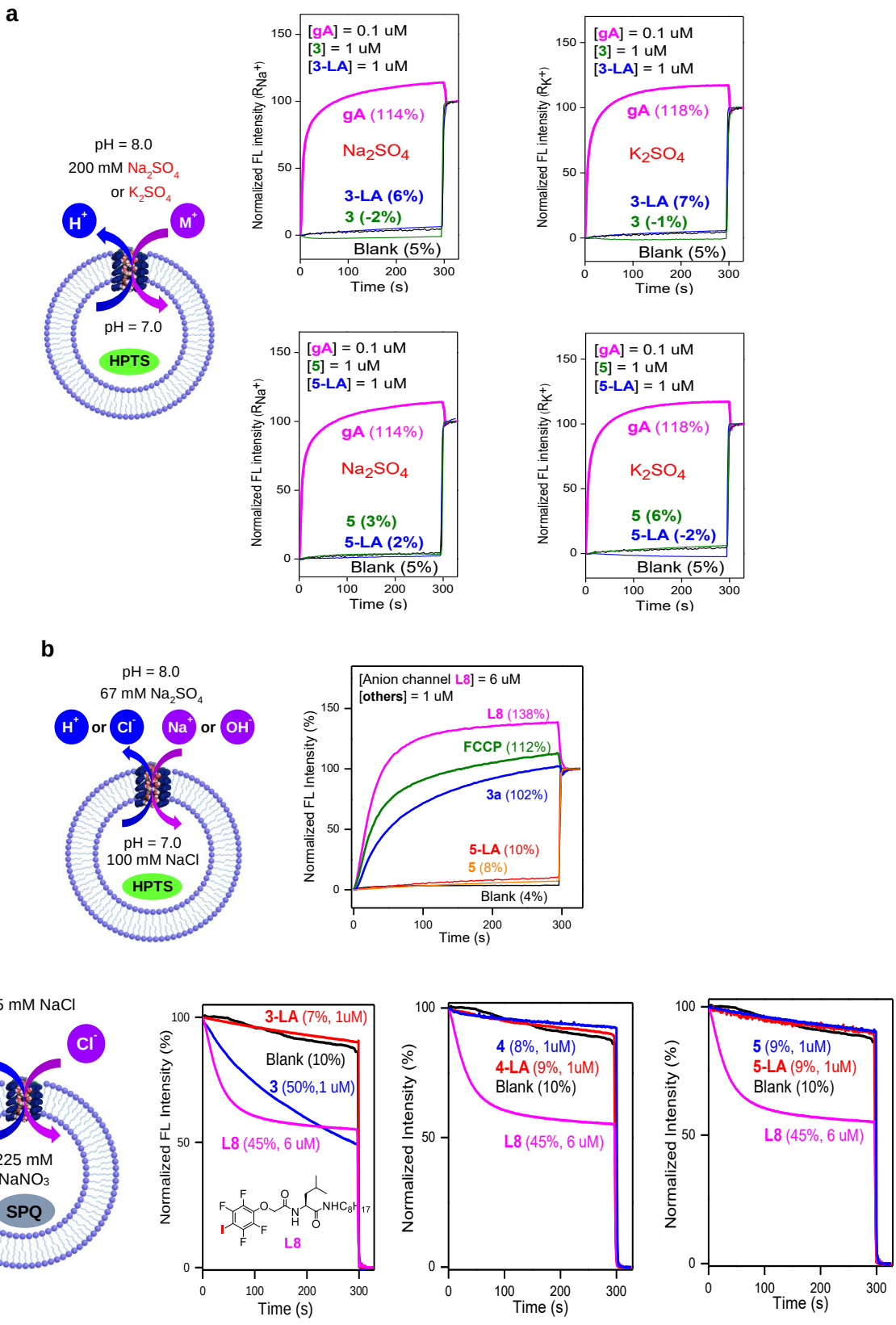

Supplementary Fig. 8 | LUV-based assays that establish low transport activities for (a) cations (Na^+ or K^+), (b) anion (Cl^-) and proton and (c) anion (Cl^-) through channels 3-5.

Estimation of Proton Transport Rate

For LUV-based ion transport scheme conducted using 2 mL buffer (10 mM HEPES, 100 mM NaCl, 0.5 mM HPTS, pH 7), see Supplementary Fig. 9a.

Proton transport rate R_p can be calculated using Eq 1.

$$R_p = N_p / t \qquad \text{Eq 1}$$

whereas N_p = number of protons transported out of LUVs, and t = transport time. N_p is correlated to the buffering capacity of the 10 mM HEPES buffer (see **Step 2** for details on the calculation)

Step 1: Given c = [LUV] = 0.13 mM, r = radius of LUV = 575 Å, s = surface area of lipid = 63.4 Å^2, n = total number of lipids per LUV, N_{LUV} = total number of LUVs per 2 mL, V_{LUV} = total internal volume of all LUVs per 2 mL, we can write Eqs 2-4

$$n = 2 * 4\pi r^2/s = 8\pi r^2/s = 130998 \qquad \text{Eq 2}$$

$$N_{LUV} = 2 \times (c \times 10^{-6} \times 6.02 \times 10^{23}) / n = 1.19 \times 10^{12} \text{ (per 2 mL)} \qquad \text{Eq 3}$$

$$V_{LUV} = N_{LUV} \times 4\pi r^3/3 \times 10^{-24} = 9.5 \times 10^{-4} \text{ mL (per 2 mL)} \qquad \text{Eq 4}$$

Step 2: Supplementary Fig. 9b provides the buffering capacity of HEPES buffer (10 mM HEPES, 100 mM NaCl, 0.5 mM HPTS, pH 7). That is, every 2.2 µL of 0.5 M NaOH is able to increase pH of 1 mL of 10 mM HEPES buffer by 0.2 pH unit. The corresponding number of OH^- ions (N_{OH}) added or H+ ions (N_H) removed per mL of buffer in order to change the pH of 1 mL buffer by 0.2 pH unit are:

$$N_H = N_{OH} = 2.2 \times 10^{-6} \times 0.5 \times 6.02 \times 10^{23} = 6.62 \times 10^{17} \qquad \text{Eq 5}$$

Step 3: Eq 5 describes the amount of H^+ or OH^- needed for changing pH by 0.2 pH unit for 1 mL of buffer, but the total volume enclosed by LUVs (V_{LUV}) is much smaller and is about 9.5×10^{-4} mL per 2 mL buffer (see Eq 4). To increase pH by 0.2 pH unit for V_{LUV}, number of protons ($N_{H(LUV)}$) to be transported from inside to outside LUVs was calculated as follow:

$$N_{H(LUV)} = \text{Eq 4} \times \text{Eq 5} = N_H \times V_{LUV} = 6.30 \times 10^{14} \text{ (per change of 0.2 pH unit for volume inside LUVs)}$$

Step 4: From ion transport activities of gA at 25 – 200 nM (Supplementary Fig 9a) and the correlation relating changes in pH to ion transport activities (Supplementary Fig. 9c), we can tabulate the following results:

Supplementary Table 7. Proton transport rate by gA at different concentrations at 50% transport activity, which corresponds to a change of 0.6 pH unit and $N_{H(LUV)}$ of 1.89×10^{14}.

Conc	Number of dimeric gA channels per 2 mL	H^+ transport activity (%)	H^+ transport Time (s)	H^+ transport rate (R_p, protons/s^{-1}) [a]	Corrected R_p [b] (protons/s^{-1})
200 nM	1.20×10^{14}	49.8	7.4	2.1	53
100 nM	6.02×10^{13}	49.8	10	3.1	78
50 nM	3.01×10^{13}	49.8	18.5	3.4	85
25 nM	1.51×10^{13}	49.8	41.5	3.0	76

[a] For instance, 2.1 = (1.89×10^{14}) / ($1.20 \times 10^{14} \times 7.4$). [b] Channel opening probability of gA is between 3% - 4%, and 4% was used to obtain corrected proton transport rate R_p (53 – 85 protons/s). These rates are comparable to the literature value of 69 protons/s at pH 7 for gA (See: *Biophys. J.* **1991**, *60*, 101-109).

Step 5: Similarly, given [**4**] = [**4-LA**] = 1 μM = 1.20 × 10^{15} molecules per 2 mL solution, and $N_{H(LUV)}$ for pH change from 7.0 to 8.0 (five 0.2 pH units) = 5 × 6.30 × 10^{14} = 3.15 × 10^{15}, if we assume ion transport of 1% over 300 s for both channels **4** and **4-LA**, proton transport rate = (3.15 × 10^{15}) × 1% / (300 × 1.20 × 10^{15}) = 8.8 × 10^{-5} protons/s. Further assuming the same channel opening probability of 4%, corrected R_p = 2.2 × 10^{-3} protons/s for both channels **4** and **4-LA**. Thus a rate of 1 × 10^{-2} protons/s can be taken as conservative estimates for both channels.

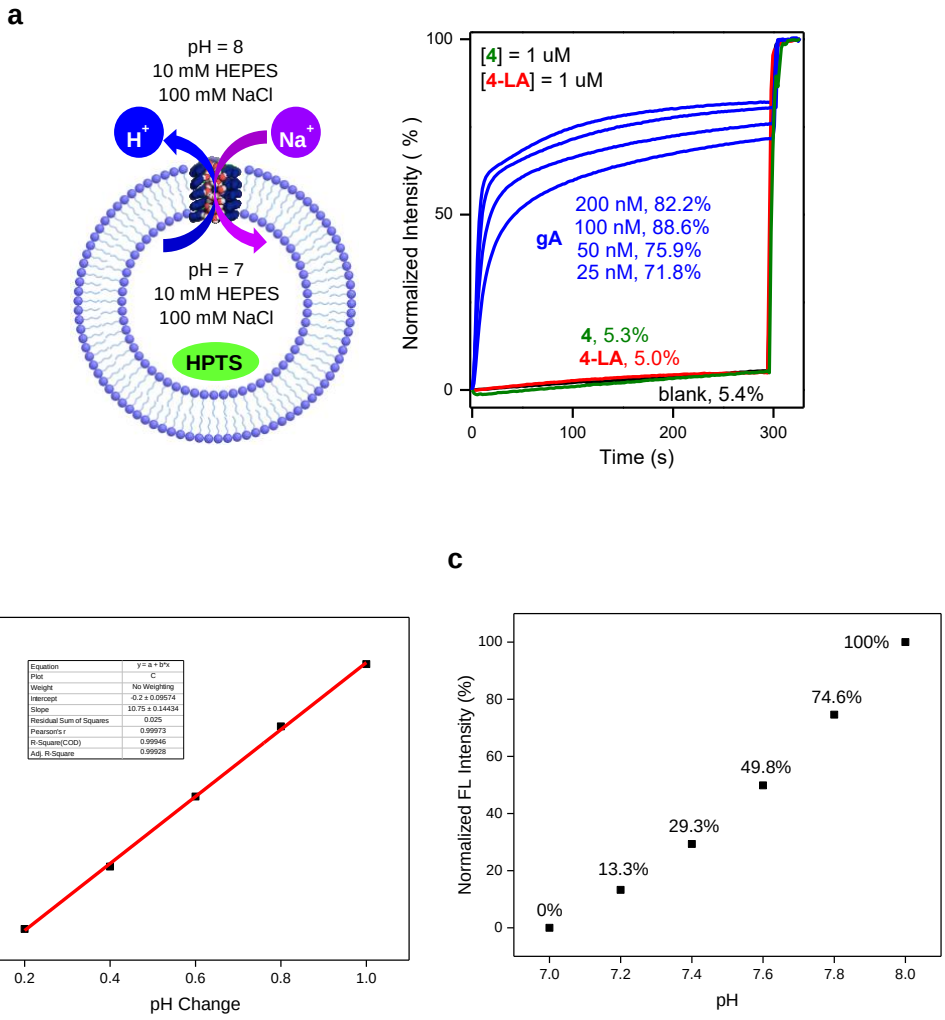

Supplementary Fig. 9 | Methods for evaluating proton transport rate by gA and channels 4 and 4-LA. a, HPTS-based assay for monitoring ion transport activities. **b**, Volume of 0.5 M NaOH needed to increase pH of 1 mL of HEPES buffer (10 mM HEPES, 100 mM NaCl and 0.5 mM HPTS) by 0.2 pH Unit. **c**, Correlation between changes in fluorescence intensity of HPTS day and changes in pH. The HPTS assay in (**a**) can also be replaced by that shown in Fig. 2e.

Measurement of proton permeation rate using stopped-flow fluorescence spectroscopy

DOPC, 3-LA reconstituted and gA reconstituted DOPC vesicles were prepared and purified using a previously described method of preparing vesicles for Cl^- permeability measurements[12] with the rehydration buffer (1 mM HPTS dyes, 10 mM HEPES, 100 mM NaCl at pH 7.0). The vesicles were mixed with the higher pH buffer solutions in the stopped-flow apparatus to impose outwardly directed H^+ gradients. Excitation wavelength of incident light was set as 454 nm and emission was measured through a band-pass filter (500/20) placed before a photomultiplier tube (PMT). Fluorescence intensity change of HPTS dyes by H^+ efflux was monitored (Supplementary Fig. 10) and this kinetic information was used to calculate proton flux of the reconstituted DOPC membranes as following.

Fluorescence intensity of HPTS dyes encapsulated by DOPC vesicles at different pH values was calibrated in the stopped-flow apparatus to obtain the correlation between fluorescence intensity and the H^+ concentration inside the DOPC vesicles (Supplementary Fig. 11). HPTS-encapsulated DOPC vesicles were prepared, mixed with different pH buffer solution, and incubated for 24 hours to equilibrate the inside and outside of H^+ concentration. After that, the fluorescence intensity was measured in the stopped-flow apparatus at fixed applied voltage of PMT (PMT HV) of 455.

$$F = a\,pH + b \quad \text{(A)}$$

F is the fluorescence intensity at fixed PMT High Voltage of 455 V, a and b are fitting constants from linear correlation between fluorescence intensity and the H^+ concentration (pH) inside the vesicles.
The first derivative of equation (A) with respect to time results in the equation (B).

$$\left.\frac{dpH}{dt}\right|_{t=0} = \frac{1}{a}\left.\frac{F}{dt}\right|_{t=0} \quad \text{(B)}$$

$\left.\frac{F}{dt}\right|_{t=0}$ was obtained by fitting the stopped-flow fluorescence traces into single-exponential fitting and used to calculate the internal pH change of vesicles. The internal H^+ concentration change by efflux of H^+ due to outwardly-directed H^+ gradients were calculated as shown in the equation (C).

$$\left.\frac{d[H^+]}{dt}\right|_{t=0} = \beta \left.\frac{dpH}{dt}\right|_{t=0} \quad \text{(C)}$$

where $\left.\frac{d[H^+]}{dt}\right|_{t=0}$ is the H^+ concentration change at $t = 0$ and β is buffer capacity. The buffer capacity is calculated using the equation (D).

$$\beta = \frac{dC}{dpH} = \frac{dC}{d[H^+]}\frac{d[H^+]}{dpH} = 2.303\left(\frac{K_w}{[H_3O^+]} + [H_3O^+] + \frac{C\,K_a[H_3O^+]}{(K_a+[H_3O^+])^2}\right) \quad \text{(D)}$$

where $[H_3O^+] = 10^{-pH}$, $K_a = 10^{-7.5}$ (HEPES buffer ions) , $K_w = 10^{-14}$, and C is the concentration of monoprotic buffer ions (HEPES).
From the left side of the equation (C), quantitative H^+ flux was calculated based on the size of vesicles under imposed $[H^+]$ gradients.

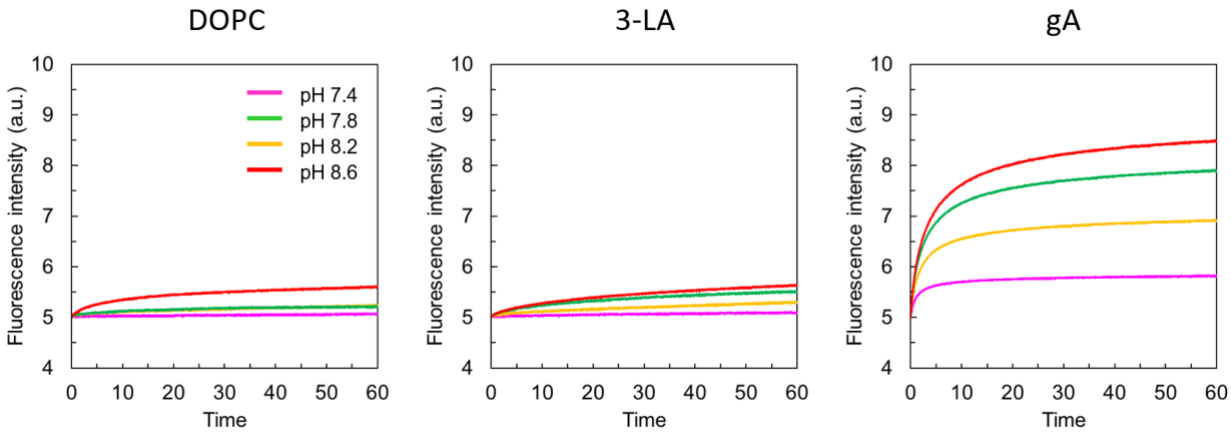

Supplementary Fig. 10 | Stopped-flow fluorescence traces for sensing proton permeation through DOPC, 3-LA reconstituted DOPC, and gA reconstituted DOPC membranes. Vesicle solutions were mixed (1:1 v/v) with different pH buffer solutions (pH 7.4, 7.8, 8.2 and 8.6) to provide to provide extravesicular pH of 7.2, 7.43, 7.58, and 7.68.

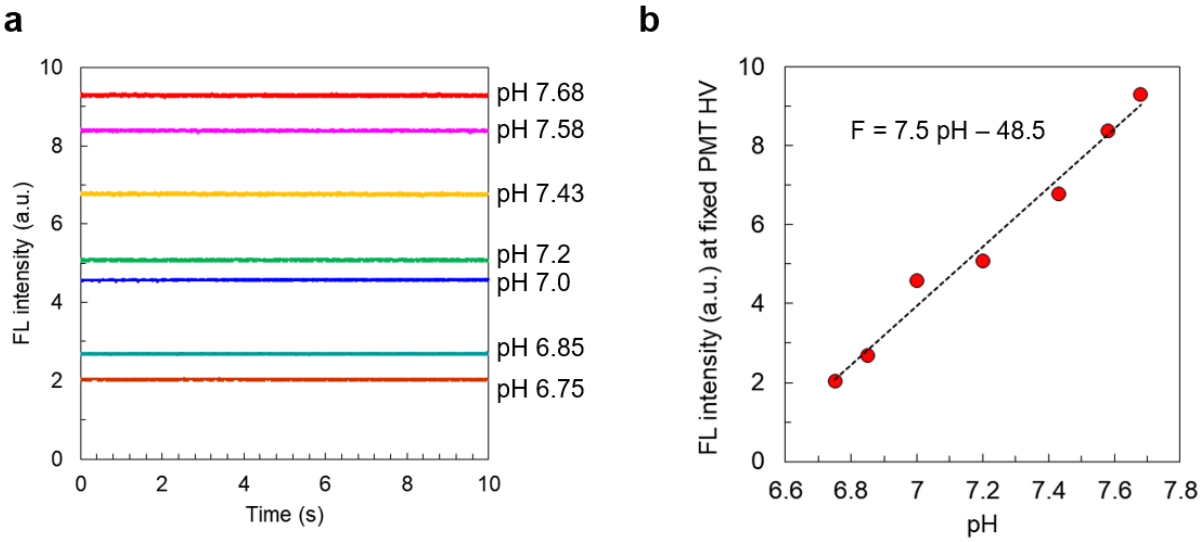

Supplementary Fig. 11 | Calibration of fluorescence intensity of HPTS dyes encapsulated by DOPC vesicles in the stopped-flow apparatus. (a) Stopped-flow fluorescence traces of the vesicles at different pH values. (b) Linear correlation between fluorescence intensity and pH values at given experimental condition. PMT HV was fixed as 455.

Discussions

Quantitative proton (H^+) permeation rate through the channels was further investigated using stopped-flow fluorescence spectroscopy. pH sensitive HPTS dyes were used as molecular probes to observe H^+ concentration change inside the reconstituted DOPC vesicles (see the experimental section and supporting information for the details of this analysis). DOPC membranes' H^+ permeability was measured as 4.9 (±6.6) $\times 10^{-4}$ cm/s (Supplementary Fig. 12), which corresponds to the range of reported proton permeability of lipid bilayer membranes[16-24]. **3-LA** and gA reconstituted DOPC vesicles were subjected to the same experiments and single-channel proton permeation rates were calculated based on the channel density in the membranes. gA channels were assumed to have 100% insertion into the membranes . At given proton concentration, gA channels transported ~10 protons per second (H^+/s) in agreement with reported gA proton permeation rates[25-27] (Supplementary Fig. 12c). For **3-LA** channels, single channel proton conduction rates were less than 0.1 H^+/s, demonstrating significantly retarded proton transport through the **3-LA** channels even at high water permeability. DOPC and **3-LA** reconstituted DOPC membranes showed nearly indistinguishable proton permeability values (error ranges overlap) when independent sets of experimental values are averaged (Supplementary Fig. 12b), demonstrating the low intrinsic proton permeability of **3-LA** channels.

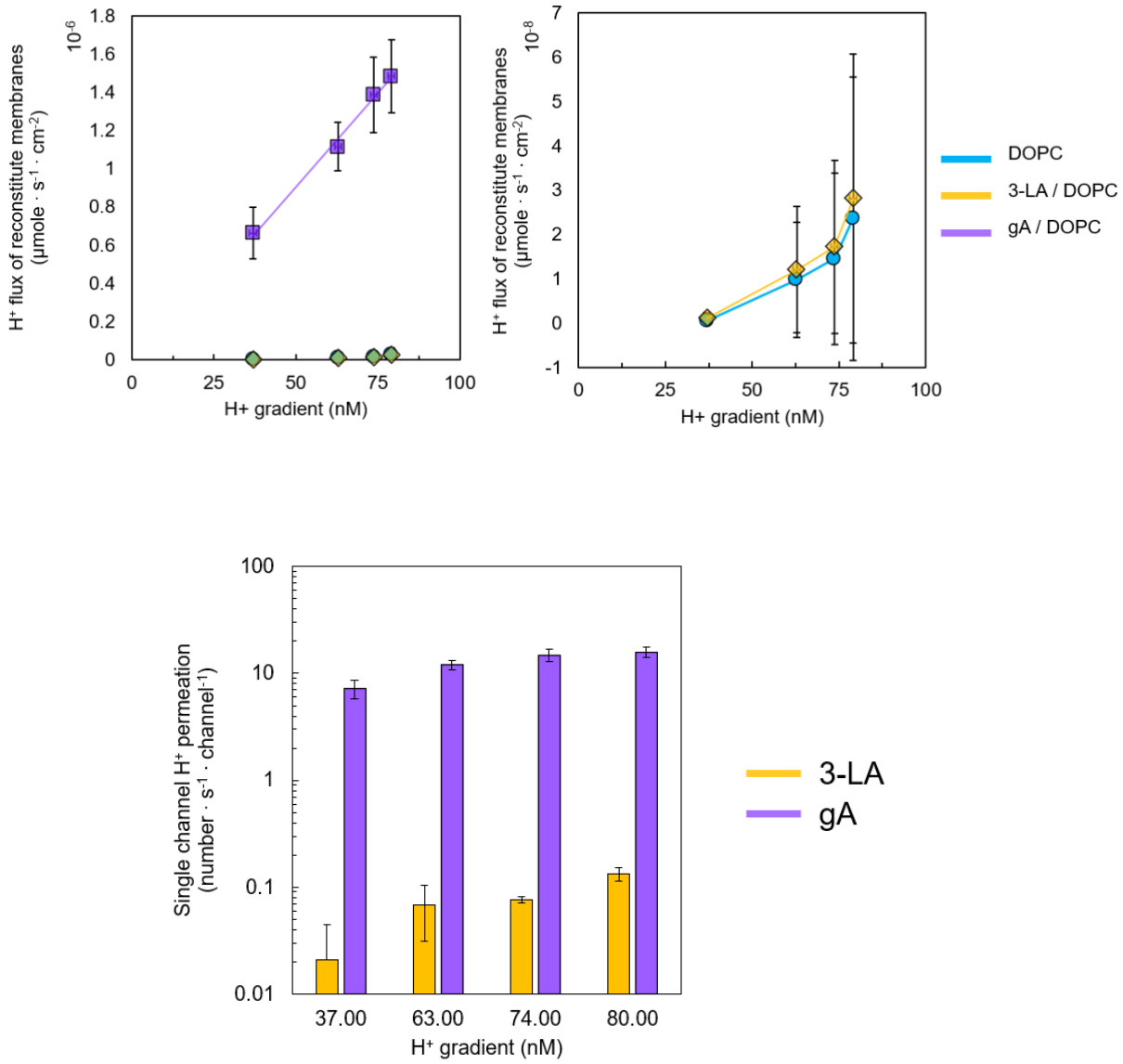

Supplementary Fig. 12 | Proton flux over the reconstituted DOPC membranes with 3-LA and gA channels (a,b) and calculated single channel proton conduction rates of 3-LA and gA channels at different pH gradients (nM) across the membranes (c).

Determination of water/Cl^- selectivity

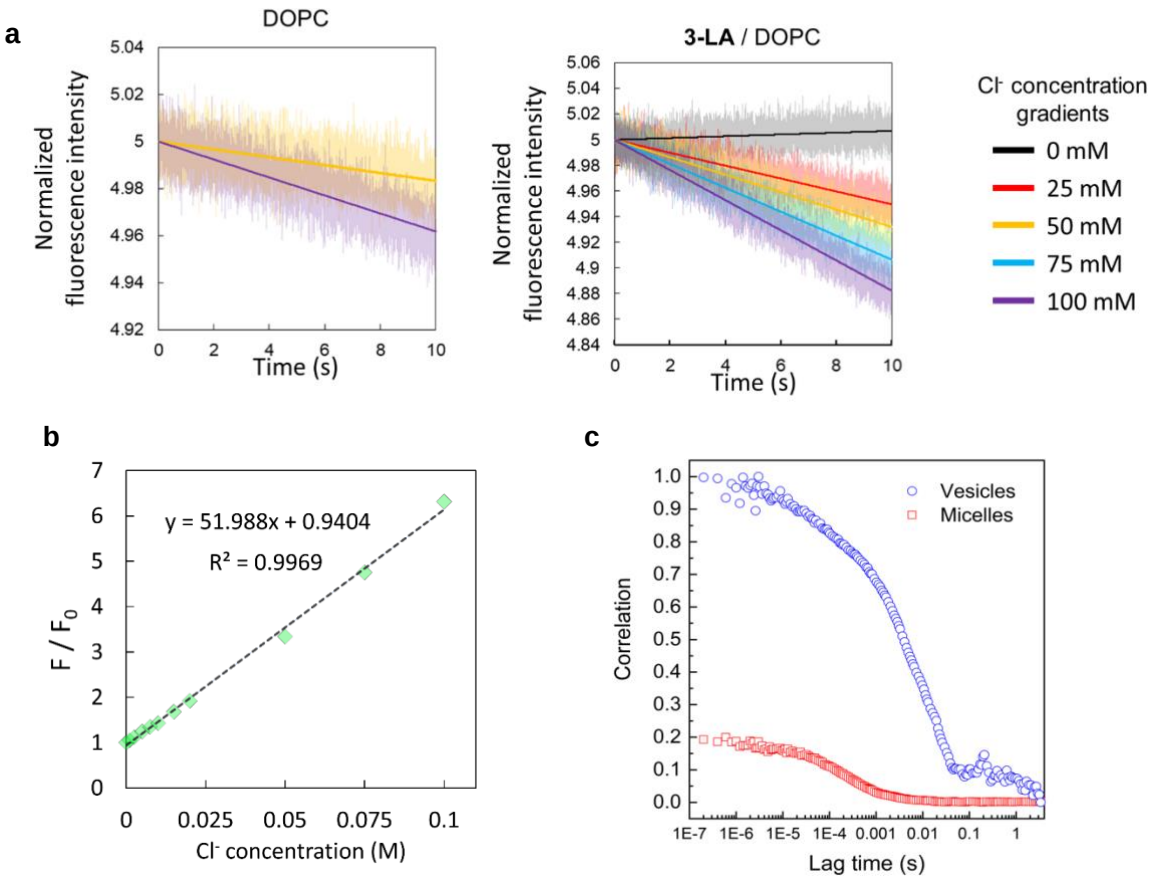

Supplementary Fig. 13 | Determination of water/Cl^- selectivity. a, Stopped-flow fluorescence traces of DOPC and **3-LA** reconstituted DOPC (**3-LA**/DOPC) vesicles that were observed at different inwardly directed Cl^- concentration gradients. Note that, for the DOPC data in the left panel, only two conditions are shown for visual clarity. **b**, Stern-Volmer plot used to determine the Stern-Volmer constant (K_{sv}) of lucigenin dyes inside DOPC vesicles. DOPC vesicles with encapsulated lucigenin dyes were prepared as described in the experimental section. The vesicles were mixed with Cl^- containing buffer so that the vesicles were exposed to different Cl^- concentration environments from 0 mM (Cl^- free) to 100 mM. After that, the samples were incubated for 24 h until the Cl^- concentration became equilibrated between inside and outside of the vesicles. The fluorescence intensity of the samples was measured using the SpectraMax M5 spectrometer, and the K_{sv} constant was extracted from the slope of the Stern-Volmer plot as shown here. As a result, K_{sv} was determined to be ~52 (1/[M]). **c**, Autocorrelation functions before and after micellizations of dye-labeled **3-LA** reconstituted DOPC vesicles that were generated from FCS experiments. The number of **3-LA** channels per vesicles were determined as 6.2 ± 4 per vesicle, which gives a number density of 2.1×10^{10} channels per cm^2 membrane area.

Molecular Dynamics Simulation for Water Transport

We constructed the all-atom models of channels **3**, **4** and **5** with LA anchors and embedded them in pre-equilibrated POPC lipid bilayer membrane. Next, we solvated them into 1M aqueous solution NaCl (Supplementary Fig. S14), and performed MD simulations as described in Methods. For the first 50 ns, the non-hydrogen atoms of the channels surrounding the transmembrane pore (but not of C_8H_{17} lipid anchors) were harmonically restrained to their initial idealized coordinate, allowing lipid molecules to adopt equilibrium configuration around the channel. The harmonic restrains were released after 50 ns, and the systems were simulated for approximately 700 ns. The hydrophobic C_8H_{17} groups were observed to radially extend away from the channel inside the lipid bilayer membrane. The channels' conformations remain closed to their initial idealized structure, with root mean squared deviation (RMSD) values stabilizing below 3 Å for channels **3-LA** and **4-LA**, and 3.5 Å for channel **5-LA** (Supplementary Fig. S14b). The area of the simulation unit cell within the plane parallels to the lipid bilayer remained constant (Supplementary Fig. S14c), suggesting that the membrane was fully equilibrated.

As soon as the simulation began, water molecules were observed to permeate through the interior cavity of the channel, from one side of the membrane to the other (Supplementary Movies S1-3). To quantify the length of the water-wires inside the channel, we calculated the number of water molecules instantaneously present inside the channel as a function of simulation time (Supplementary Fig. S15a). The distribution of the number of water molecules calculated from the simulation trajectory suggests that the most probable number of water molecules contained in channels **3-LA** and **4-LA** are 48 and 33, respectively. To understand the mechanism of water transport in these channels, we calculated the number of hydrogen bonds (H-bonds) and proton-wire breakers among the water molecules present inside the channels. Supplementary Figs. S15b, 15c and 16 show the total number of H-bonds and proton wire-breakers with respect to the simulation time. There are approximately two H-bonds per water molecules inside both the channels. Among the water molecules inside the channel, close to 36% tend to break the proton wire.

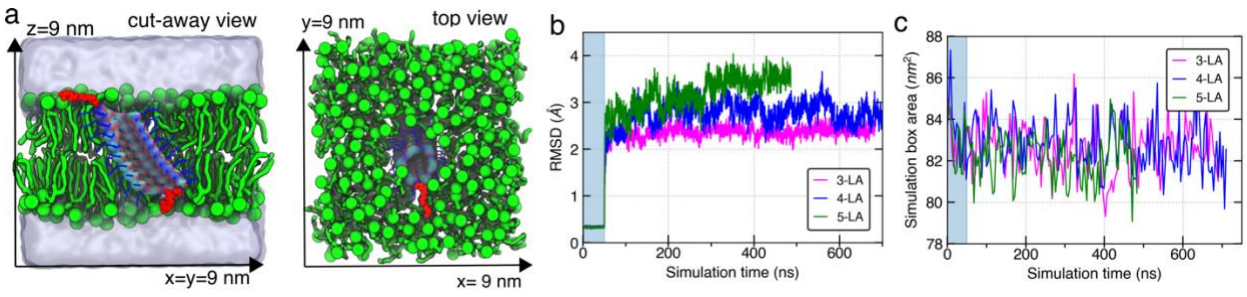

Supplementary Fig. 14 | All-atom model and simulation of membrane spanning AWCs. a, A representative snapshot of the simulated system: cut-away side view and a top view of channel **3-LA** embedded in a POPC lipid bilayer membrane and solvated in 1 M NaCl solution. A carbon atom of the amine-group of each POPC molecule is shown as a large green sphere, whereas the rest of each molecule is shown as a thick green line. The channel is shown using a molecular surface representation. The lipid anchoring alkyl chains (C_8H_{17}) of the channel are shown in licorice blue. The LA anchors at the ends of the channels are shown in red. The volume occupied by the electrolyte solution is represented by a semi-transparent surface. **b,** The RMSD of the channels' coordinates from that of their idealized initial conformation as a function of simulation time. The RMSD was computed for all non-hydrogen atoms of the foldamer scaffold (excluding flexible C_8H_{17} and LA anchors) after aligning each frame to the initial model. **c,** The area of the simulation box in x-y plane as a function of simulation time. The blue shaded region shows the time when channels were restrained using harmonic constraints.

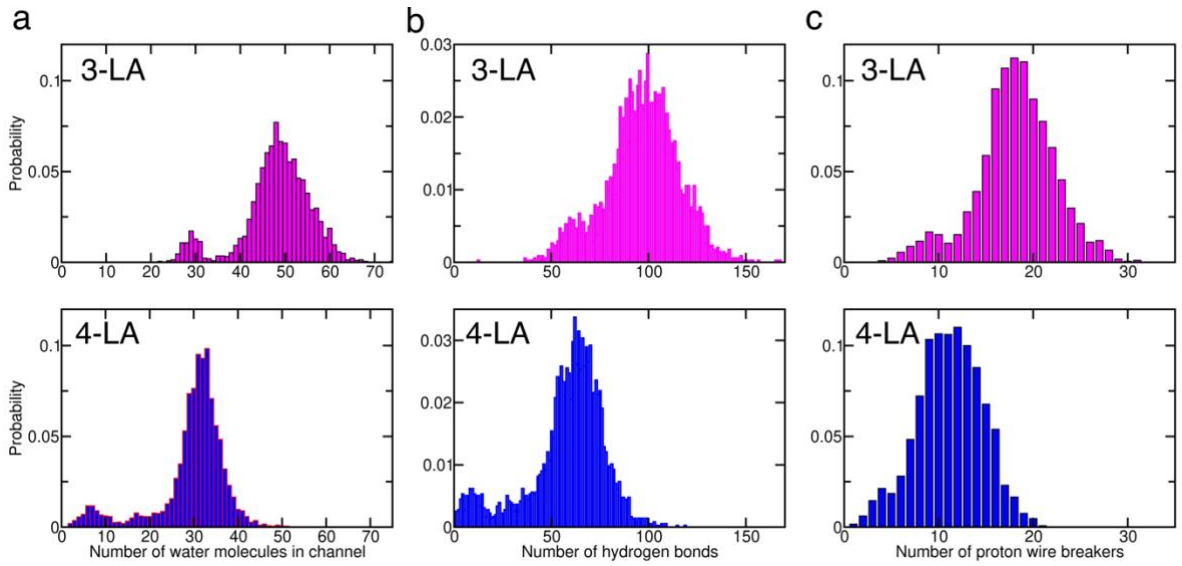

Supplementary Fig. 15 | The histograms. a, The total number of water molecules present inside the channels **3-LA** and **4-LA**. **b,** Hydrogen bonds among the water molecules inside the channels. **c,** The total number of proton-wire breaking water molecules inside the channels. The histograms were obtained from the MD simulation trajectories as shown in Supplementary movies SM1 and SM2.

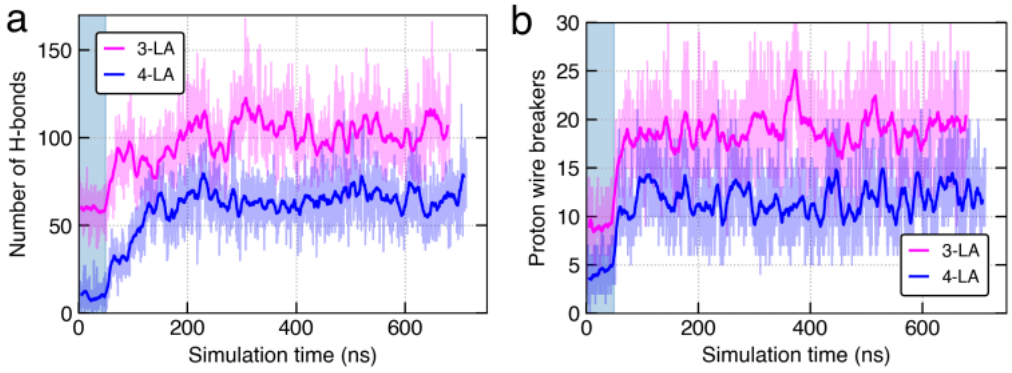

Supplementary Fig. 16 | H-bonds and proton wire breakers inside channels 3-LA and **4-LA**. **a,** The total number of H-bonds formed between the water molecules present inside channels **3-LA** and **4-LA** as a function of simulation time. **a,** The total number of water molecules breaking the proton-wire inside the channels **3-LA** and **4-LA** as a function of simulation time.

Proton Wire Breakers inside Channel 3

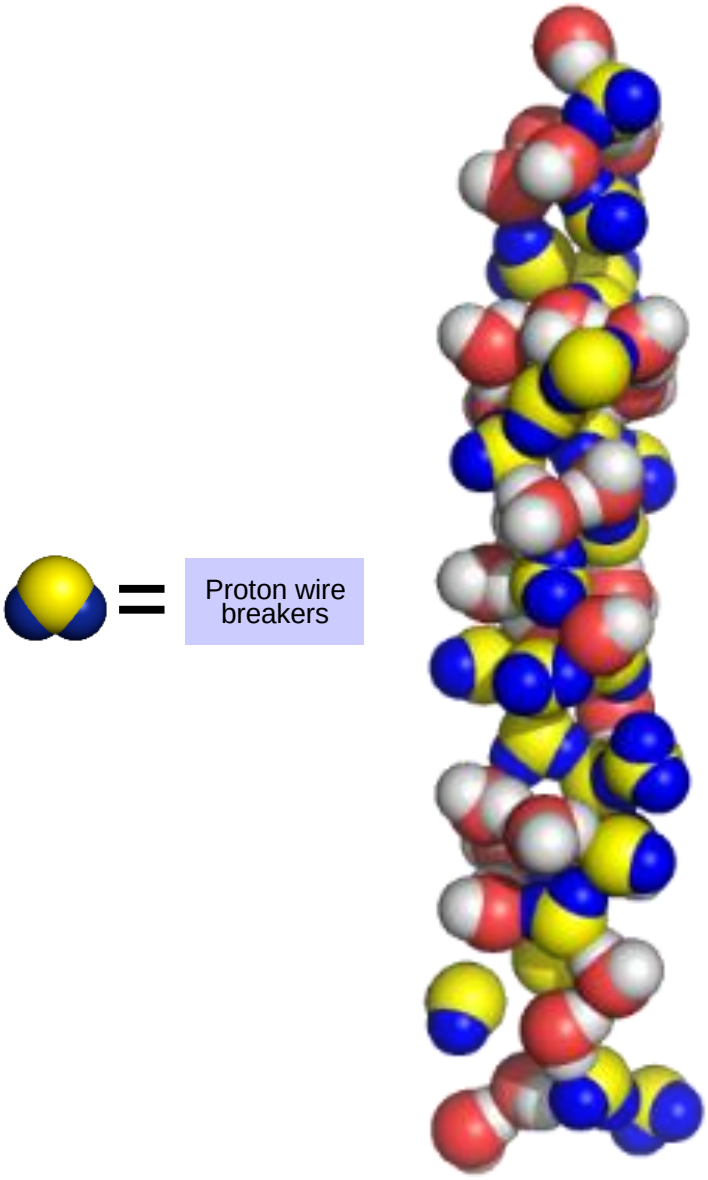

Proton wire breakers inside **3**

Supplementary Fig. 17 | One MD snapshot of LA-containing channel 3, having 26 units 1 and 25 units 2 and a height of 2.9 nm, illustrating 26 proton wire breakers and 27 regularly H-bonded water molecules. These proton wire breakers block proton transport that would occur via the Grotthuss mechanism, leading to high rejection of protons observed for channels **3** and **3-LA**.

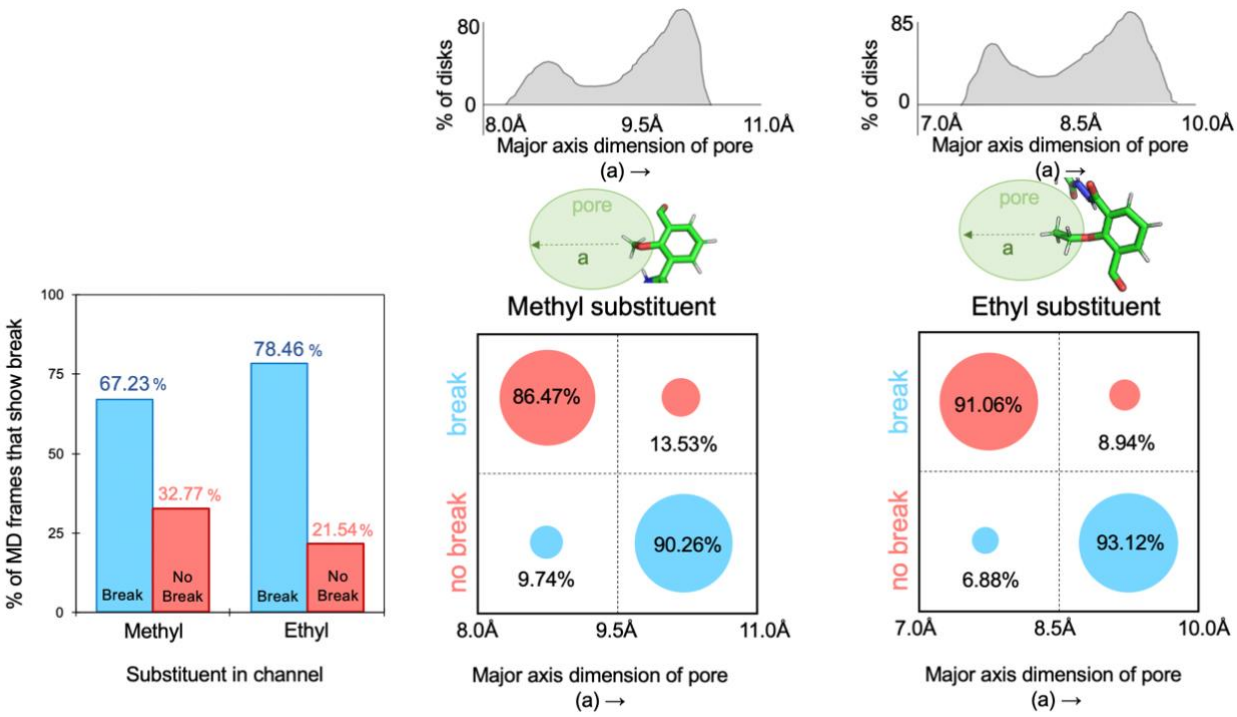

Supplementary Fig. 18 | Analysis of MD simulation trajectories to elucidate the effect of fluctuating methyl and ethyl groups on creating defects (breaks) in proton wires, leading to exclusion of proton permeation across channels 3-LA and 4-LA. The left panel shown that a majority of the frames for the methyl and ethyl substituted channels show a break in the proton wire. Mid and right panels show that for both the methyl and ethyl substituted channels the reduced channel dimension correlates with a break in the proton wire.

Supplementary movies

Supplementary movies**,** SM1 and SM2 and SM3, show 700 ns, 750 ns, and 500 ns long all-atom equilibrium MD simulation trajectory of **3-LA**, **4-LA** and **5-LA** channels respectively. A cut-away view of the system is presented to illustrate the transmembrane water permeation. A carbon atom of the amine-group of each POPC molecule is shown as a large green sphere, whereas the rest of each molecule is shown as a thick green line. The channel is shown using a molecular surface representation. The lipid anchoring alkyl chains (C_8H_{17}) of the channel are shown in licorice blue. The LA anchors at the ends of the channels are shown in yellow spheres. The water molecules inside and near the channels are shown using red (oxygen) and white (hydrogen) spheres. The rest of the water and ions are not shown in the movies.

Free-energy and H-bond analysis of MD trajectories

To elucidate the mechanism of water transport through **3-LA**, **4-LA**, and AQP1 channels, we computed the average number of hydrogen bonds formed by the water molecules inside each channel and between these molecules and the channel's walls (Supplementary Figure S19a-c). First, we identified all water molecules present inside each channel for each frame of the equilibration trajectory. The inner volume of **3-LA**, and **4-LA** was defined to lie within 5 Å from the nitrogen atoms of the **3-LA** or **4-LA** walls (for AQP, within 5 Å from the nitrogen atoms of the peptide backbone), and within the membrane, abs(z) < 20 Å. Then, we computed the total number of hydrogen bonds formed by these water molecules along themselves and with the channel walls and divided those two numbers by the number of water molecules to obtain average number of H-bons per water molecule. A hydrogen bond was defined using a 3.5 Å cut off for the donor--acceptor distance and a 45° cut off for the donor-hydrogen-acceptor angle. On average, a water molecule was found to form a greater number of hydrogen bonds with the walls of AQP1 (1.6 H-bonds) as compared to the walls of **3-LA** and **4-LA** (0.8 H-bonds).

To estimate the energetics of water permeation through **3-LA**, **4-LA**, and AQP1, we determined the potential of mean force (PMF) of a single water molecule within each channel using the replica exchange umbrella sampling method, [28,29] Eighty one replicas of each channel system were created differing by the coordinate of one restrained water molecule, spanning the +/- 40 Å range along the bilayer normal (z-axis) in 1 Å bins. The initial coordinates for the replicas were taken from a trajectory of a water molecule passing through the respective channel during the equilibration simulation. The 81 replicas were simulated in parallel for approximately 75, 50, and 25 ns for the **3-LA**, **4-LA**, and AQP1 system, respectively, having the z-coordinate of the water molecule restrained to the centre of the sampling window with the spring constant of 2.5 kcal/mol/ Å^2. During the simulation, the replicas were allowed to exchange the biasing potential between the neighbouring windows with a probability given by the Metropolis algorithm. Finally, we used the weighted histogram analysis method[30] to subtract the contribution from the confining harmonic potential and extract the free energy profile. The error of the PMF calculation was estimated by splitting the sampling data sets into two halves, computing the PMF for each half and using the absolute difference of the two PMFs in each window as a measure of the error. Figure S19d shows the free energy profile of a water molecule as a function of its z-coordinate in the respective channel. The water molecule faces a lower barrier in AQP1 (~1 kcal/mol) as compared to **3-LA** and **4-LA** (~3 kcal/mol).

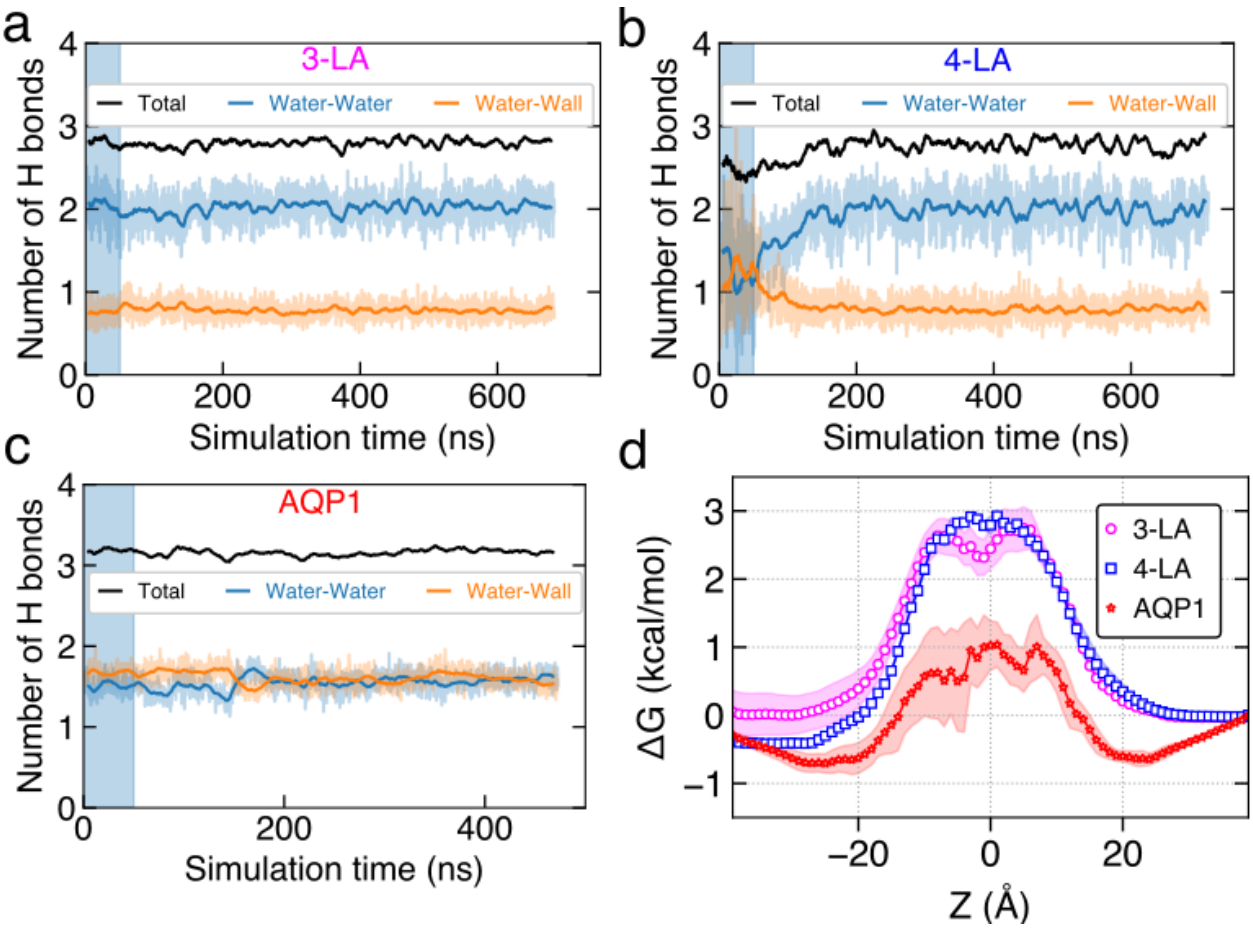

Supplementary Fig. 19 | H-bond and free-energy analysis of MD trajectories. a-c, The number of intermolecular H-bonds per water molecule among the water molecules confined to the channel, and between the water molecules within the channel and the channel's inner walls. Solid lines show a 10-ns moving average of a 200-ps sampled data (faded lines in background). **d,** The free energy of a water molecule inside the **3-LA**, **4-LA** and AQP1 channel as a function of the molecule's z-coordinate. The shadowed regions illustrate the estimated errors of the free-energy calculation. **a**-**d**. Taking 5.1 kcal/mol as the H-bond energy and each water forming four H-bonds in bulk water, the activation energies can be estimated to be 6.1, 6.3 and 4.1 kcal/mol for **3-LA**, **4-LA** and AQP1, respectively, values that are consistent with their respective experimental activation energies of 8.7, 8.3 and 5.0 kcal/mol.

$^{1}H/^{13}C$ NMR Spectra:

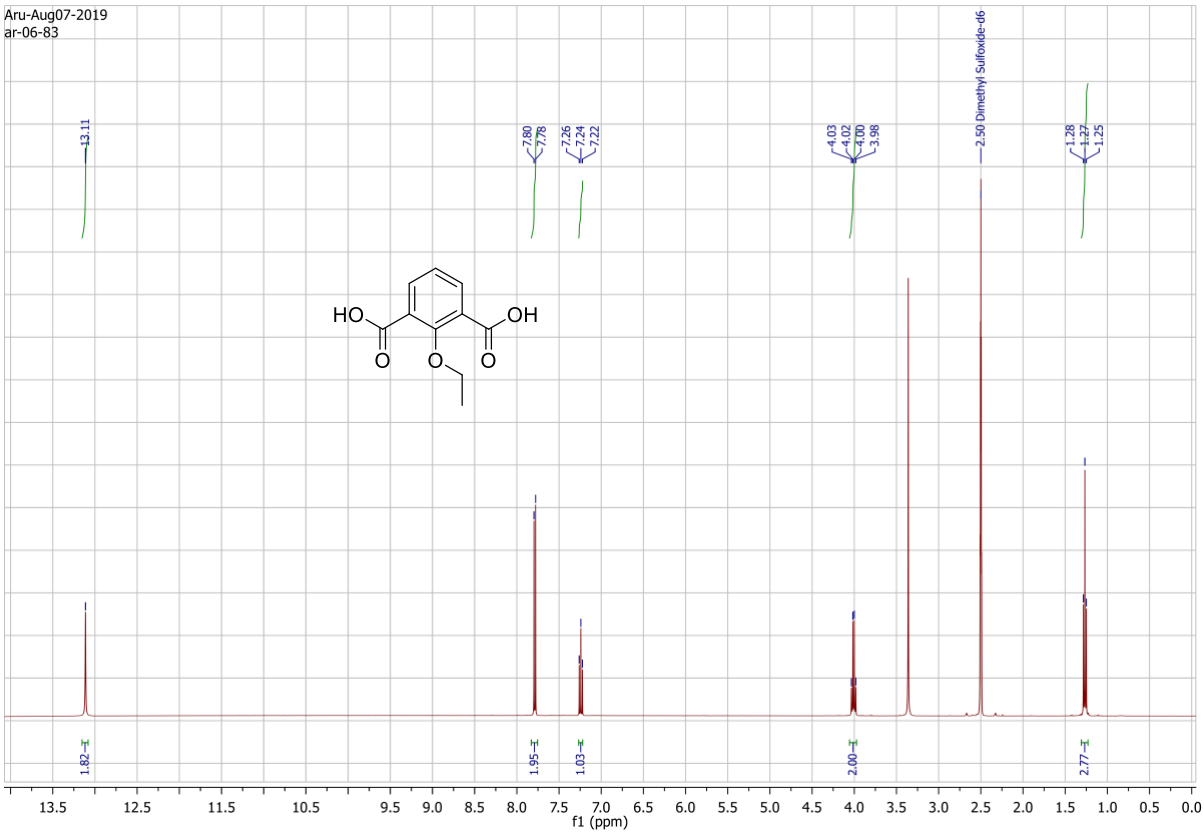

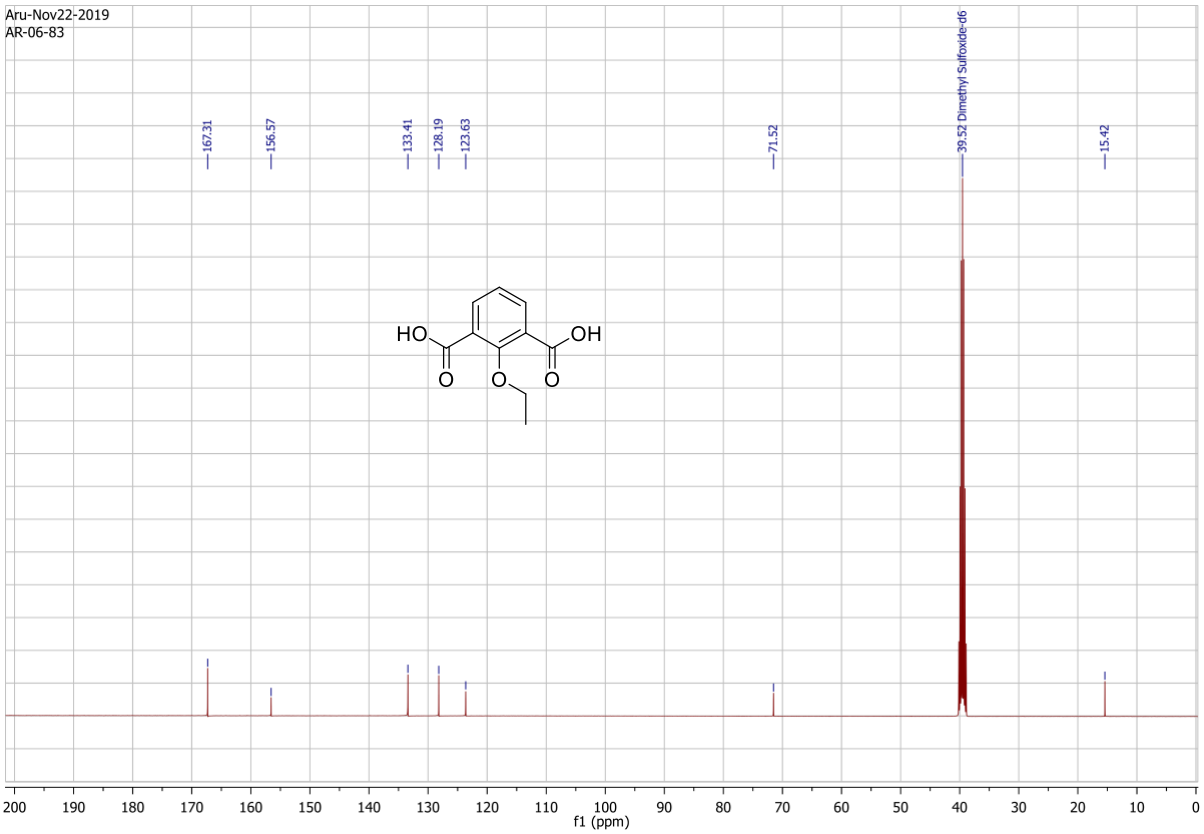

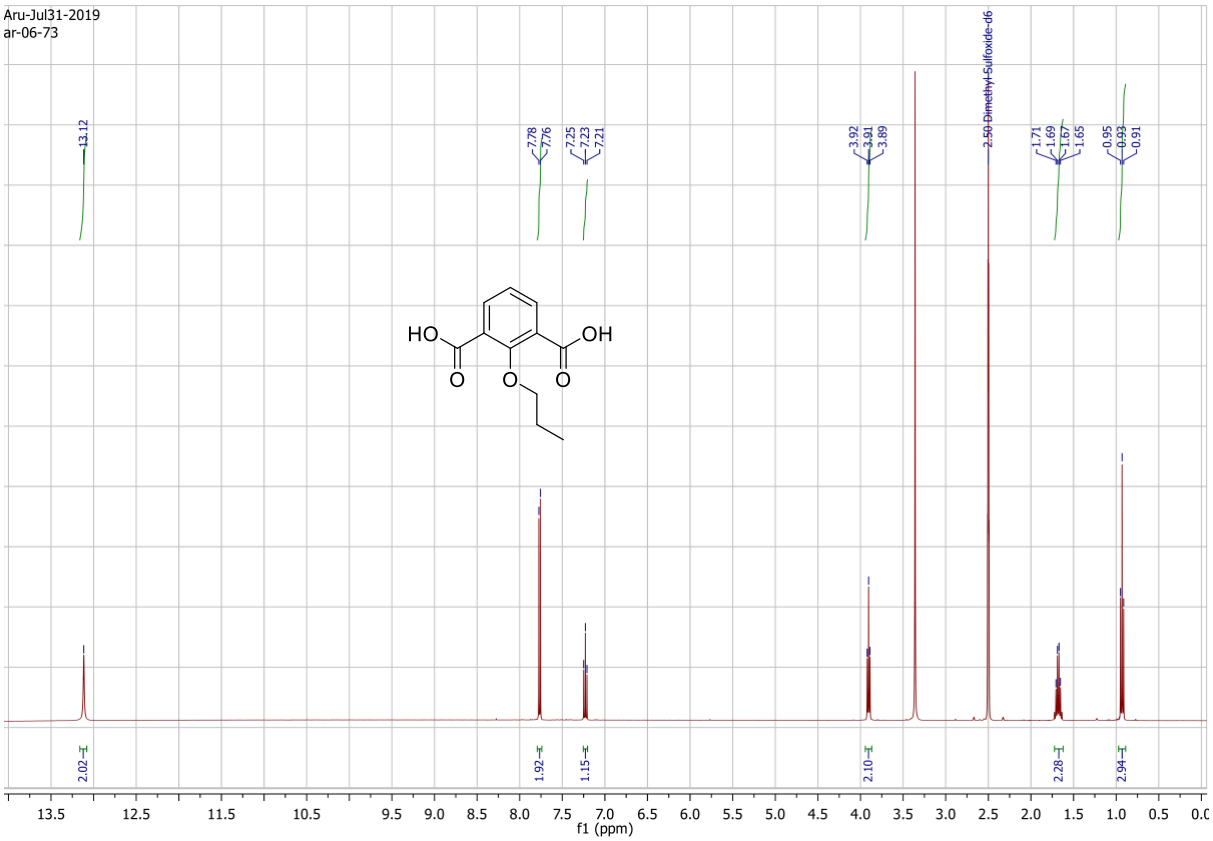
Aru-Jul31-2019
ar-06-73
13.12
7.78
7.76
7.25
7.23
7.21
3.92
3.91
3.89
2.50 Dimethyl-Sulfoxide-d6
1.71
1.69
1.67
1.65
0.95
0.93
0.91
HO
OH
O
O
O
2.02
1.92
1.15
2.10
2.28
2.94
f1 (ppm)

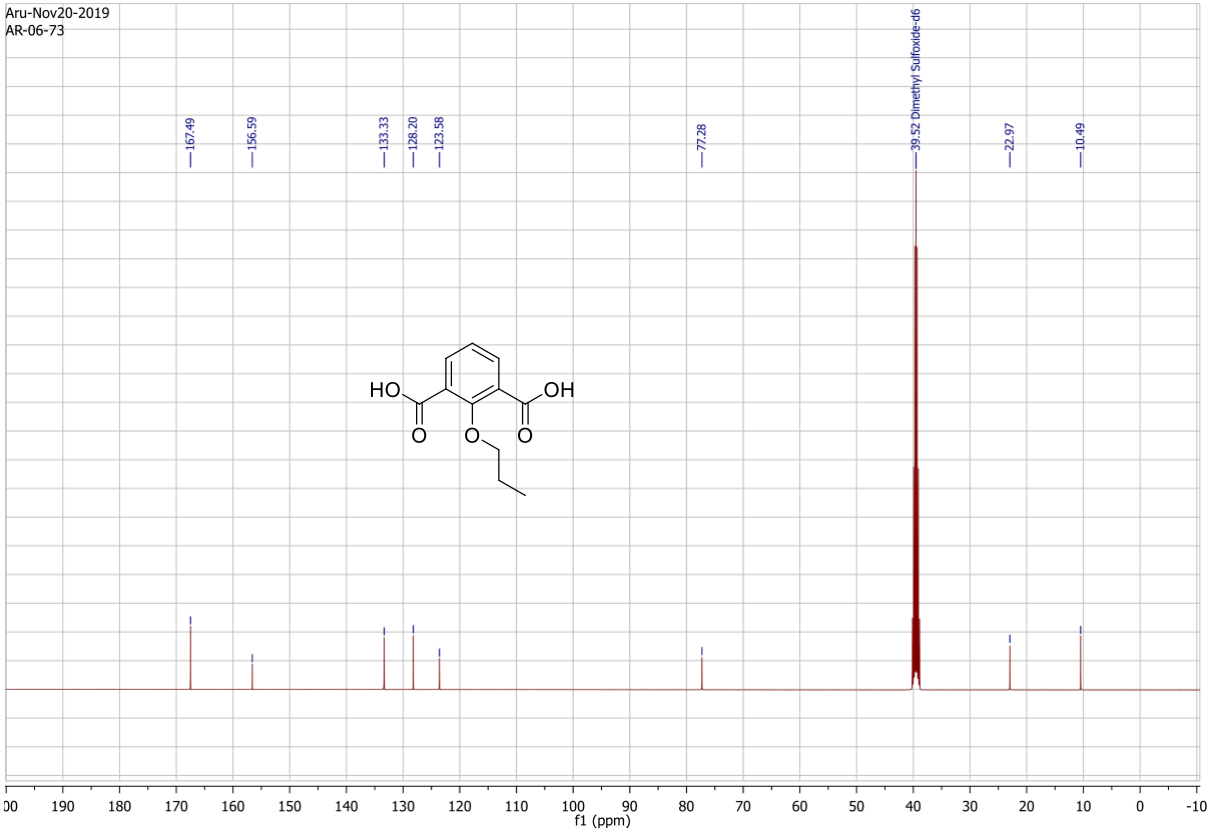
Aru-Nov20-2019
AR-06-73
167.49
156.59
133.33
128.20
123.58
77.28
39.52 Dimethyl Sulfoxide-d6
22.97
10.49
HO
OH
O
O
O
f1 (ppm)

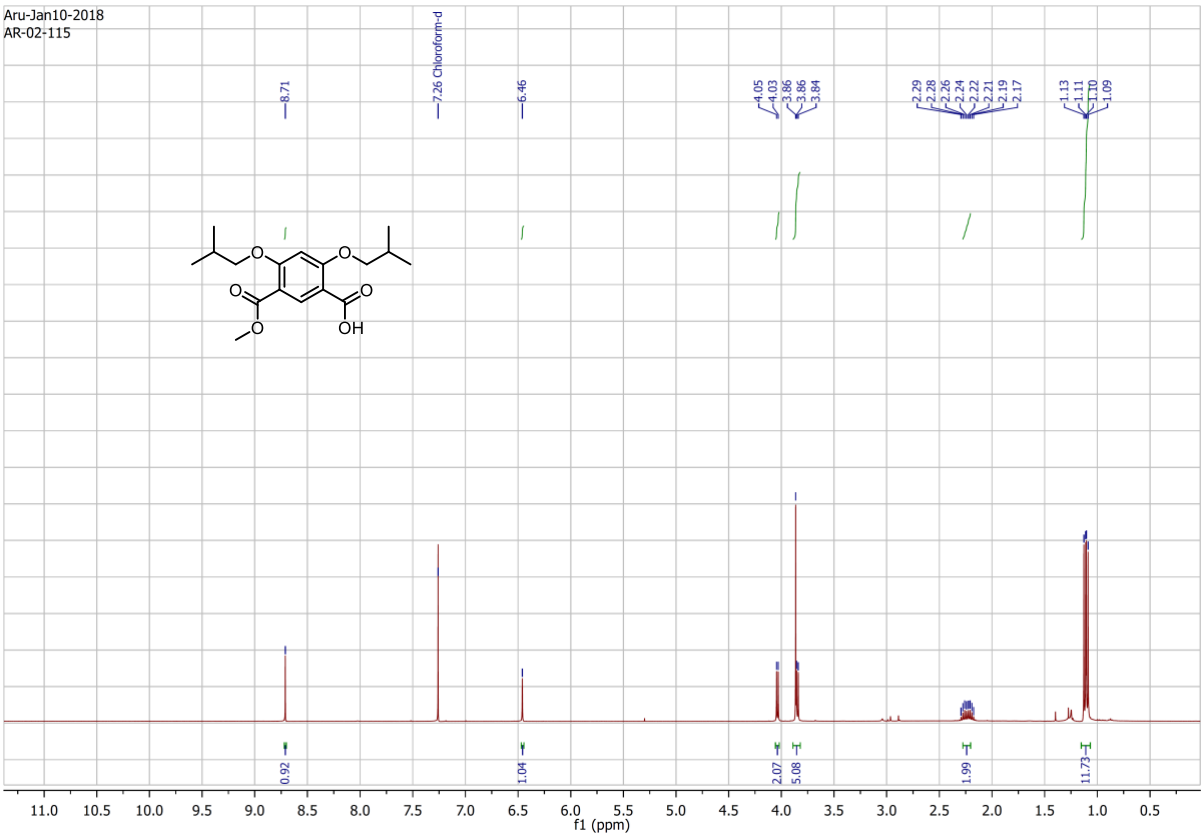
Aru-Jan10-2018
AR-02-115
8.71
7.26 Chloroform-d
6.46
4.05
4.03
3.86
3.86
3.84
2.29
2.28
2.26
2.24
2.22
2.21
2.19
2.17
1.13
1.11
1.10
1.09
O
O
O
O
O
OH
0.92
1.04
2.07
5.08
1.99
11.73
11.0
10.5
10.0
9.5
9.0
8.5
8.0
7.5
7.0
6.5
6.0
5.5
5.0
4.5
4.0
3.5
3.0
2.5
2.0
1.5
1.0
0.5
f1 (ppm)

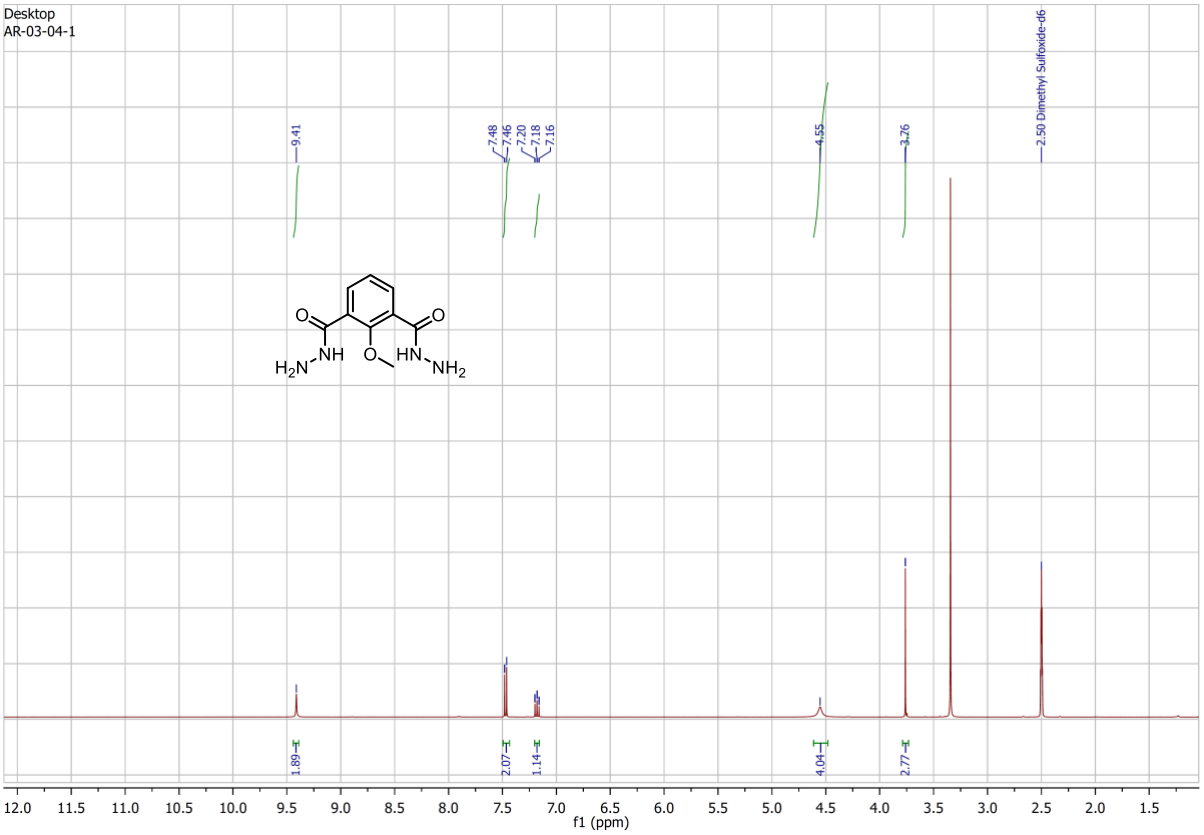
Desktop
AR-03-04-1
9.41
7.48
7.46
7.20
7.18
7.16
4.55
3.76
2.50 Dimethyl Sulfoxide-d6
O
O
O
H2N
NH
HN
NH2
1.89
2.07
1.14
4.04
2.77
12.0
11.5
11.0
10.5
10.0
9.5
9.0
8.5
8.0
7.5
7.0
6.5
6.0
5.5
5.0
4.5
4.0
3.5
3.0
2.5
2.0
1.5
f1 (ppm)

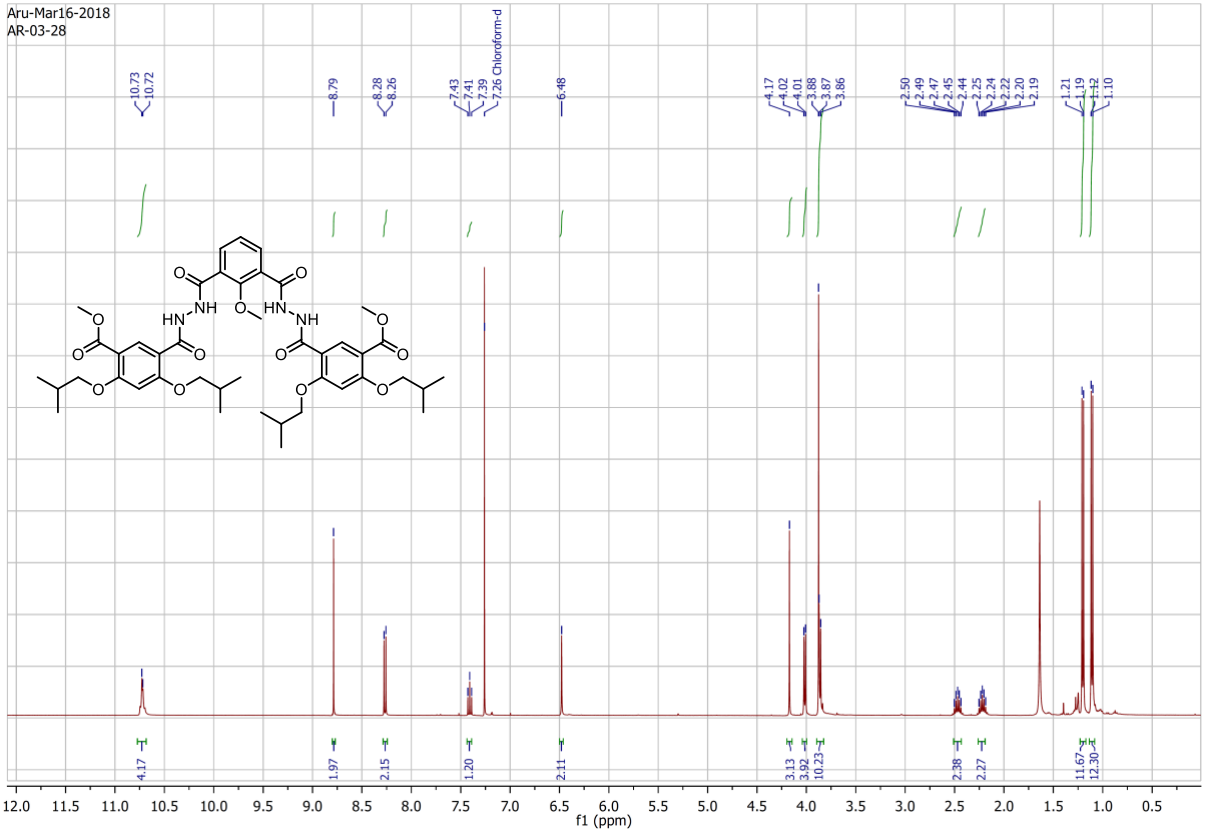

References:

1. Komati, R. *et al.* Tenacic Acids: A New Class of Tenacious Binders to Metal Oxide Surfaces. *Chem. Eur. J.* **24**, 14824-14829 (2018).
2. Roy, A. *et al.* Polyhydrazide-Based Organic Nanotubes as Efficient and Selective Artificial Iodide Channels. *Angewa. Chem. Int. Ed.* **n/a**.
3. Zhong, D.-C., Liao, L.-Q., Wang, K.-J., Liu, H.-J. & Luo, X.-Z. Heat-set gels formed from easily accessible gelators of a succinamic acid derivative (SAD) and a primary alkyl amine (R-NH2). *Soft Matter* **11**, 6386-6392 (2015).
4. Bie, F., Wang, Y., Shang, J., Gallagher, N. M. & Jiang, H. Synergistic Recognition of Halide Anions and Saccharides by Oligohydrazide Foldamers. *Eur. J. Org. Chem.* **2013**, 8135-8144 (2013).
5. You, L.-Y., Wang, G.-T., Jiang, X.-K. & Li, Z.-T. Hydrogen bonded aromatic hydrazide foldamers for the self-assembly of vesicles and gels. *Tetrahedron* **65**, 9494-9504 (2009).
6. Tunuguntla, R. H. *et al.* Enhanced water permeability and tunable ion selectivity in subnanometer carbon nanotube porins. *Science* **357**, 792-796 (2017).
7. Shen, Y.-X. *et al.* Achieving high permeability and enhanced selectivity for Angstrom-scale separations using artificial water channel membranes. *Nat. Commun.* **9**, 2294 (2018).
8. Tang, C. Y., Zhao, Y., Wang, R., Hélix-Nielsen, C. & Fane, A. G. Desalination by biomimetic aquaporin membranes: Review of status and prospects. *Desalination* **308**, 34-40 (2013).
9. Schneider, S. *et al.* Columnar Self-Assemblies of Triarylamines as Scaffolds for Artificial Biomimetic Channels for Ion and for Water Transport. *J. Am. Chem. Soc.* **139**, 3721-3727 (2017).

10. Horner, A. *et al.* The mobility of single-file water molecules is governed by the number of H-bonds they may form with channel-lining residues. *Sci. Adv.* **1**, e1400083 (2015).
11. Hannesschläger, C., Barta, T., Siligan, C. & Horner, A. Quantification of Water Flux in Vesicular Systems. *Sci. Rep.* **8**, 8516 (2018).
12. Song, W. *et al.* Artificial water channels enable fast and selective water permeation through water-wire networks. *Nat. Nanotechnol.* **15**, 73-79 (2020).
13. Licsandru, E. *et al.* Salt-Excluding Artificial Water Channels Exhibiting Enhanced Dipolar Water and Proton Translocation. *J. Am. Chem. Soc.* **138**, 5403-5409 (2016).
14. Roy, A. *et al.* Self-assembly of small-molecule fumaramides allows transmembrane chloride channel formation. *Chem. Commun.* **54**, 2024-2027 (2018).
15. Ren, C. *et al.* A halogen bond-mediated highly active artificial chloride channel with high anticancer activity. *Chem. Sci.* **9**, 4044-4051 (2018).
16. Chander, A., Grabe, M., Moore, H. P. and Machen, T. E. Proton leak and CFTR inregulation of Golgi pH in respiratory epithelial cells. *Am. J. Physiol. Cell Physiol.* **281**, C908-C921 (2001).
17. Gutknecht, J. Proton conduction through phospholipid bilayers: water wires or weak acids? *J. Bioenerg. Biomembr.* **19**, 427-442 (1987).
18. Lande, M. B., Donovan, J. M. and Zeidel, M. L. The relationship between membrane fluidity and permeabilities to water, solutes, ammonia, and protons. *J. Gen. Physiol.* **106**, 67-84 (1995).
19. Miedema, H., Staal, M. and Prins, H. B. pH-induced proton permeability changes of plasma membrane vesicles. *J. Membr. Biol.* **152**, 159-167 (1996).
20. Nichols, J. W. and Deamer, D. W. Net proton-hydroxyl permeability of large unilamellar liposomes measured by an acid-base titration technique. *Proc. Natl. Acad. Sci. USA* **77**, 2038-2042 (1980).
21. Norris, F. A. and Powell, G. L. Characterization of CO_2/carbonic acid mediated proton flux through phosphatidylcholine vesicles as model membranes. *Biochim. Biophys. Acta* **1111**, 17-26 (1992).
22. Nozaki, Y. and Tanford C. Proton and hydroxide ion permeability of phospholipid vesicles. *Proc. Natl. Acad. Sci. USA* **76**, 4324-4328 (1981).
23. Paula, S., Volkov, A. G., Van, H. A. N., Haines, T. H. and Deamer, D. W. Permeation of protons, potassium ions, and small polar molecules through phospholipid bilayers as a function of membrane thickness. *Biophys. J.* **70**, 339-348 (1996).
24. Perkins, W. R. and Cafiso, D. S. An electrical and structural characterization of H^+/OH^- currents in phospholipid vesicles. *Biochemistry* **25**, 2270-2276 (1986).
25. Decoursey, T. E. Voltage-gated proton channels and other proton transfer pathways. P*hysiol. Rev.* **83**, 475-579 (2003).
26. Deamer, D. W. Proton permeation of lipid bilayers. *J. Bioenerg. Biomembr.* **19**, 457-479 (1987).
27. Song, W. et al. Artificial water channels enable fast and selective water permeation through water-wire networks. *Nat. Nanotechnol.* **15**, 73-79 (2020).
28. Sugita, Y., Kitao, A., Okamoto, Y. Multidimensional replica-exchange method for free-energy calculations. *J. Chem. Phys.* **113**, 6042-6051 (2000).
29. Roy, A., Joshi, H., Ye, R. J., Shen, J., Chen, F., Aksimentiev, A., Zeng, H. Q. Polyhydrazide-Based Organic Nanotubes as Efficient and Selective Artificial Iodide Channels. *Angew. Chem. Int. Ed.* **59**, 4806-4813 (2020).

30. Kumar, S., Rosenberg, J. M., Bouzida, D., Swendsen, R. H., Kollman, P. A. The weighted histogram analysis method for free-energy calculations on biomolecules. I. The method. *J. Comput. Chem.* **13**, 1011-1021 (1992).